Angewandte Chemie
Eine Zeitschrift der Gesellschaft Deutscher Chemiker

Supporting Information

Reactivities of Interstitial Hydrides in a Cu_{11} Template: En Route to Bimetallic Clusters

Rhone P. Brocha Silalahi, Qi Wang, Jian-Hong Liao, Tzu-Hao Chiu, Ying-Yann Wu, Xiaoping Wang, Samia Kahlal, Jean-Yves Saillard, and C. W. Liu**

anie_202113266_sm_miscellaneous_information.pdf
anie_202113266_sm_cif.zip
anie_202113266_sm_SI.xyz

Supplementary Information

Experimental Section

Materials and Measurement

All the reactions were carried out under an N_2 atmosphere by using the standard Schlenk technique. The solvents used in this work were distilled before use, following standard protocols. All chemicals were purchased from different commercial sources available and used as received. $[Cu_{11}H_2\{S_2P(O^iPr)_2\}_6(C{\equiv}CPh)_3]$,[1] $[Cu(CH_3CN)_4](PF_6)$,[2] $[Ag(CH_3CN)_4](PF_6)$,[3] $Au(PPh_3)Cl$,[4] and $[NH_4][S_2P(O^iPr)_2]$[5] were prepared by following the procedures reported in literatures. NMR spectra were recorded on a Bruker Avance DPX-300 FT-NMR spectrometer that operates at 300 MHz while recording ^1H, 121.5 MHz for ^{31}P, and 46.1 MHz for ^2H. ^{109}Ag NMR spectrum was recorded on a Bruker AV-600 BBO probe, operating at 27.918 MHz. Used residual solvent proton references: δ, $CDCl_3$, 7.26 and δ, d_6-acetone, 2.10. The $^{31}P\{^1H\}$ NMR spectra were referenced to external 85% H_3PO_4 at δ = 0.00 ppm. The chemical shift (δ) and coupling constants (J) are reported in ppm and Hz, respectively. ESI-mass spectra were recorded on a Fison Quattro Bio-Q (Fisons Instruments, V.G. Biotech, U. K.). UV–Visible absorption spectra were measured on a Perkin Elmer Lambda 750 spectrophotometer using quartz cells with a path length of 1 cm. An Edinburgh FLS920 spectrophotometer recorded the PL excitation and emission spectra with the Xe 900 lamp as the excitation source. The PL at 77 K was recorded in an EPR tube with a Cold Finger Dewars Flask. The PL decays were measured using an Edinburgh FLS920 spectrometer with a gated hydrogen arc lamp using a scatter solution to profile the instrument response function.

Synthesis of [1·PF_6]

Cluster **1** can be prepared by the following two methods.

Method A: In a flame-dried Schlenk tube, $[Cu_{11}H_2\{S_2P(O^iPr)_2\}_6(C{\equiv}CPh)_3]$ (**H_2Cu_{11}**) (0.05 g; 0.0219 mmol) was added to a flask along with 10 mL acetone solvent; then $[Cu(CH_3CN)_4](PF_6)$ (0.0082 g; 0.0219 mmol) was added under vigorous stirring. The reaction was aged 10 minutes under N_2 atmosphere at room temperature. The solvent was evaporated under vacuum, and the residue was washed with methanol to remove impurities. The orange residue continued to dissolve in acetone, and the solvent was evaporated to dryness under vacuum to get a pure orange powder of $[CuH_2Cu_{11}\{S_2P(O^iPr)_2\}_6(C{\equiv}CPh)_3](PF_6)$ (**1**). Yield: 0.044 g, 95%, based on Cu. Similarly, the deuterium analog of **1**, $[CuD_2Cu_{11}\{S_2P(O^iPr)_2\}_6(C{\equiv}CPh)_3](PF_6)$ was

synthesized by using $[Cu_{11}D_2\{S_2P(O^iPr)_2\}_6(C{\equiv}CPh)_3]$ (0.05 g; 0.0219 mmol) in place of $[Cu_{11}H_2\{S_2P(O^iPr)_2\}_6(C{\equiv}CPh)_3]$. Yield: 0.040 g, 84.9% , based on Cu.

Methods B: In a flame-dried Schlenk tube, $[NH_4][S_2P(O^iPr)_2]$ (0.046 g; 0.2 mmol) and $[Cu(CH_3CN)_4](PF_6)$ (0.149 g, 0.4 mmol) were dissolved in mixed solvent CH_3CN and THF (*v/v* =1/1). To this mixture, HC≡CPh (40 uL; 0.4 mmol) and NEt_3 (40 uL; 0.4 mmol) were added, and the reaction mixture was stirred at 32ºC for 10 minutes. $NaBH_4$ (0.0038 g; 0.1 mmol), was added to this reaction mixture and stirred for 3 hours under an N_2 atmosphere. The solvent was evaporated under vacuum and residue washed with hexane (3×15 mL) to remove unreacted alkyne. The orange residue was washed with methanol (3×15 mL) to remove $[Cu_8H\{S_2P(O^iPr)_2\}_6]^+$ and subsequently dissolved in acetone. Then the solvent was evaporated to dryness under vacuum to get a pure orange powder of $[CuH_2Cu_{11}\{S_2P(O^iPr)_2\}_6(C{\equiv}CPh)_3](PF_6)$ (**1**) (Yield: 0.023 g, 28.2 % based on Cu). Similarly, the deuterium analog of **1** of $[CuD_2Cu_{11}\{S_2P(O^iPr)_2\}_6(C{\equiv}CPh)_3](PF_6)$ (0.0245 g, 29.5 % based on Cu) was synthesized by using $NaBD_4$ (0.0048 g; 0.1 mmol) in place of $NaBH_4$.

($\mathbf{1_H}$): ESI-MS: *m/z* at 2346.41 (calcd. 2346.42) for $[Cu_{12}H_2\{S_2P(O^iPr)_2\}_6(C{\equiv}CPh)_3]^+$ $(\mathbf{1_H})^+$. ^{1}H NMR (300 MHz, d_6-acetone): 7.46-7.74 (15 H, - C_6H_5), 5.24 (2*H*, μ$_4$-H), 4.87-5.13 (12 H, *CH*), 1.29-1.45 (72 H, CH_3) ppm. $^{31}P\{^1H\}$ NMR (121.49 MHz, d_6-acetone): 99.5 (s, S_2P) and -143.0 (sept., PF_6^-). FT-IR data in KBr pellet (cm^{-1}): 2997.3, 2952.4, 2877.3, 2016.2, 1728.1, 1585.6, 1460.0, 1169.2, 1145.8, 1069.4, 960.9, 862.5, 766.7, 691.8. Anal. Calcd. for $C_{60}H_{101}Cu_{12}F_6O_{12}P_7S_{12}$: C, 28.91 ; H, 4.08; S, 15.43. Found: C, 29.18; H, 4.25; S, 15.33.

($\mathbf{1_D}$): ESI-MS: *m/z* at 2348.37 (calc. 2348.42) for $[Cu_{12}D_2\{S_2P(O^iPr)_2\}_6(C{\equiv}CPh)_3]^+$ $(\mathbf{1_D})^+$. ^{1}H NMR (300 MHz, d_6-acetone): 7.46-7.74 (15 H, -C_6H_5), 4.85-5.14 (12 H, *CH*), 1.29-1.45 (72 H, CH_3) ppm. ^{2}H NMR (46.1 MHz, acetone): 5.29 (2D, μ$_4$-D) ppm. $^{31}P\{^1H\}$ NMR (121.49 MHz, d_6-acetone): 99.5 (s, S_2P) and -143.0 (sept., PF_6^-) ppm. FT-IR data in KBr pellet (cm^{-1}): 2996.1, 2960.9, 2871.3, 2016.4, 1725.2, 1570.4, 1464.3, 1169.0, 1145.6, 1069.5, 924.2, 865.1, 765.9, 691.8.

Synthesis of [2·PF6]

In a flame-dried Schlenk tube $[Cu_{11}H_2\{S_2P(O^iPr)_2\}_6(C{\equiv}CPh)_3]$ (**H_2Cu_{11}**) (0.05 g; 0.0219 mmol) was added to a flask along with 10 mL acetone solvent; then $[Ag(CH_3CN)_4](PF_6)$ (0.009 g; 0.0219 mmol) was added under vigorous stirring. The reaction was aged 10 minutes under N_2 atmosphere at room temperature. The solvent was evaporated under a vacuum, and the residue was washed with hexane and ether (3×15 mL) to remove impurities. The black residue was dissolved with methanol to get a black solution. Then, the solvent was evaporated to dryness

under vacuum to get a pure black powder of $[AgH_2Cu_{14}\{S_2P(O^iPr)_2\}_6(C{\equiv}CPh)_6](PF_6)$ (**2**). Yield: 0.020 g, 24.6 %, based on Cu.

Similarly, the deuterium analog of **2**, $[AgD_2Cu_{11}\{S_2P(O^iPr)_2\}_6(C{\equiv}CPh)_6](PF_6)$ (Yield: 0.019 g, 23.3 %, based on Cu) was synthesized by using $[Cu_{11}D_2\{S_2P(O^iPr)_2\}_6(C{\equiv}CPh)_3]$ (0.05 g; 0.0219 mmol) in place of $[Cu_{11}H_2\{S_2P(O^iPr)_2\}_6(C{\equiv}CPh)_3]$.

(2H): ESI-MS: *m/z* at 2883.76 (calc. 2884.26) for $[AgH_2Cu_{14}\{S_2P(O^iPr)_2\}_6(C{\equiv}CPh)_6]^+$ $(\mathbf{2_H})^+$. ^{1}H NMR (300 MHz, d_6-acetone): 7.49-7.76 (30 H, -C_6H_5), 5.15 (2H, μ_5-H; ($^1J(^1H\text{-}^{107}Ag)$ = 93.6 Hz, $^1J(^1H\text{-}^{109}Ag)$ = 107.7 Hz)), 4.80-5.04 (12 H, *CH*), 1.01-1.45 (72 H, CH_3) ppm. ^{109}Ag NMR (27.918 MHz, d_6-acetone): 1279.5 ppm (t, $^1J(^1H\text{-}^{109}Ag)$ = 107.7 Hz). $^{31}P\{^1H\}$ NMR (121.49 MHz, d_6-acetone): 101.4 (s, S_2P) and -143.0 (sept., PF_6^-) ppm. FT-IR data in KBr pellet (cm^{-1}): 2978.4, 2933.5, 2872.3, 2003.6, 1718.3, 1570.5, 1464.0, 1177.8, 1069.6, 972.1, 886.4, 756.9, 690.0. No satisfactory elemental anaylsis data can be acquired due to the decomposition of cluster **2**.

(2D): ESI-MS: *m/z* at 2554.33 (calc. 2554.32) for $[AgD_2Cu_{14}\{S_2P(O^iPr)_2\}_6(C{\equiv}CPh)_6\text{-}\{CuC{\equiv}CPh\}_2]^+$. ^{1}H NMR (300 MHz, d_6-acetone):7.47-7.74 (30 H, -C_6H_5), 4.86-4.94 (12 H, *CH*), 1.12-1.43 (72 H, CH_3) ppm. ^{2}H NMR (46.1 MHz, THF): 5.15 (2D, μ_5-D; ($^1J_{DAg}$ = 15.4 Hz)) ppm, $^{31}P\{^1H\}$ NMR (121.49 MHz, d_6-acetone): 101.4 (s, S_2P) and -143.0 (sept., PF_6^-) ppm.

Synthesis of [3]

In a flame-dried Schlenk tube $[Cu_{11}H_2\{S_2P(O^iPr)_2\}_6(C_2Ph)_3]$ (**H_2Cu_{11}**) (0.05 g; 0.0219 mmol) was added to a flask along with 10 mL acetone solvent; then $Au(PPh_3)Cl$ (0.01g; 0.0219 mmol) was added under vigorous stirring. The reaction was aged 10 minutes under N_2 atmosphere at room temperature. The solvent was evaporated under vacuum, and the residue dissolved in hexane. The orange solution was evaporated to dryness under vacuum to get a pure orange powder of $[AuCu_{11}\{S_2P(O^iPr)_2\}_6(C{\equiv}CPh)_3Cl]$ (**3**). Yield: 0.025 g, 45%, based on Cu.

(3): ESI-MS: *m/z* at 2478.43 (caclc. 2478.40) for $[AuCu_{11}\{S_2P(O^iPr)_2\}_6(C{\equiv}CPh)_3\text{-}Cl]^+$ [**3**-Cl]$^+$. ^{1}H NMR (300 MHz, d_6-acetone):7.55-7.73 (15 H, -C_6H_5), 4.86-5.23 (12 H, *CH*), 1.33-1.44 (72 H, CH_3) ppm. $^{31}P\{^1H\}$ NMR (121.49 MHz, d_6-acetone): 97.8 (s, S_2P) ppm. FT-IR data in KBr pellet (cm^{-1}): 2989.4, 2953.4, 2870.0, 1967.4, 1736.3, 1569.2, 1463.2, 1174.0, 1140.6, 1069.4, 942.2, 861.3, 763.5, 697.0. No satisfactory elemental anaylsis data can be acquired due to the decomposition of cluster **3**.

Synthesis of $[4]^+$

In a flame-dried Schlenk tube $[AuCu_{11}\{S_2P(O^iPr)_2\}_6(C{\equiv}CPh)_3Cl]$ (0.1 g; 0.04 mmol) and [CuC≡CPh] (0.007g; 0.04 mmol) were added to a flask along with 10 mL acetone. The reaction was aged 10 minutes under N_2 atmosphere at room temperature. The solvent was evaporated under a vacuum, and the residue was washed with CH_2Cl_2/water (3x15 mL). The CH_2Cl_2 layer separated, then red solution was evaporated to dryness under vacuum to get a pure red powder of $[AuCu_{12}\{S_2P(O^iPr)_2\}_6(C{\equiv}CPh)_4]^+$ ($[\mathbf{4}]^+$).[7] Yield: 0.05 g, 46%, based on Cu.

[4]$^+$: ESI-MS: *m/z* 2642.23 (calc. 2642.37) for $[AuCu_{12}\{S_2P(O^iPr)_2\}_6(C{\equiv}CPh)_4]^+$ $[\mathbf{4}]^+$. ^{1}H NMR (400 MHz, $CDCl_3$): 7.60-7.61 (20H, C_6H_5), 4.82 (12H, OC*H*), 1.12 (72H, CH_3) ppm; $^{31}P\{^1H\}$ NMR (121.49 MHz, $CDCl_3$); 101.7 (s, S_2P) ppm.

Synthesis of [5·PF_6]

In flame-dried Schlenk tube, $[Cu_{20}H_{11}\{S_2P(O^iPr)_2\}_9]$[6] (0.1 g, 0.031 mmol) was suspended in THF (5 mL) along with $[Ag(CH_3CN)_4](PF_6)$ (0.013 g, 0.031 mmol) and phenylacetylene (40 µL, 0.341 mmol). The resulting mixture was stirred at 30°C for 72 hours. The solvent was evaporated under vacuum. The obtained precipitate was washed with diethyl ether (3x15 mL) to remove impurities from the ligand. The dark residue was extracted in methanol and pass through Al_2O_3. Finally, the solvent was evaporated to dryness under vacuum to get a pure dark purple powder of $[Ag@Cu_{12}\{S_2P(O^iPr)_2\}_6(C{\equiv}CPh)_4](PF_6)$ (**5**). In this reaction, corresponding alkenes and $[Cu_8H\{S_2P(O^iPr)_2\}_6](PF_6)$ have been produced as byproducts. Yield: 0.025 g, 19.27%, based on Cu.

(**5**) ESI-MS: *m/z* at 2554.25 (caclc. 2552.31) for $[AgCu_{12}\{S_2P(O^iPr)_2\}_6(C{\equiv}CPh)_4]^+$ $(\mathbf{5})^+$. ^{1}H NMR (300 MHz, d_6-acetone): 7.47-7.73 (20H, C_6H_5), 4.90 (12H, OC*H*), 1.15-1.43 (72H, CH_3) ppm. $^{31}P\{^1H\}$ NMR (121.49 MHz, d_6-acetone); 100.2 (s, S_2P) and -143.0 (sept., PF_6^-) ppm.

Single-Crystal X-ray Crystallography

The single crystals of **1**-**3** were mounted on the tip of a glass fiber coated with paratone oil, then frozen. Data were collected on a Bruker APEX II CCD diffractometer using graphite monochromated Mo Kα radiation (λ = 0.71073 Å) at 150 (**1, 3**) and 100 K (**2**). Absorption corrections for the area detector were performed with SADABS,[8] and the integration of raw data frame was performed with SAINT.[9] The structure was solved by direct methods and refined by least-squares against F^2 using the SHELXL-2018/3 package,[10, 11] incorporated in SHELXTL/PC V6.14.[12] All non-hydrogen atoms were refined anisotropically. The hydride

atoms were located from the residual electron densities and refined without constraints in cluster **1**. In cluster **2**, the hydrides (H2M) were refined with distance constraints between metal and hydrogen. In the cluster **2**, both of the two oxygen atoms on P1 and one phenyl ring on C78 were found disordered over two positions with 75% and 25% occupancy. One phenyl ring on C70 was found disordered over two positions with 65% and 35% occupancy. Two carbon atoms on C43 were found disordered over two positions with the same occupancy. In cluster **3**, one of the isopropoxy groups on P1, Cl1 atom and Cu11 were found disordered over two positions with 70% and 30% occupancy. The structure reported herein has been deposited at the Cambridge Crystallographic Data Centre, CCDC no. 2095375 (**1·PF$_6$**), 2095376 (**2·PF$_6$**), and 2095378 (**3**).

Single-Crystal Neutron Diffraction

The hydride locations in **2** were confirmed by a single-crystal neutron diffraction experiment using the TOPAZ single-crystal neutron time-of-flight (TOF) Laue diffractometer at ORNL's Spallation Neutron Source (structure **2$_N$**).[13] Single crystals suitable for neutron diffraction were obtained by slowly diffusing hexane into a concentrated acetone solution (2:1 volume) at -4°C for 12 days. A dark red block-shaped crystal (2.90 mm × 3.75 mm × 4.20 mm) was attached to a MiTeGen loop using a perfluorinated grease (Krytox GPL 205) and cooled 20 K with a Cryomech P415 pulse tube cryocooler for data collection. A total of 13 crystal orientations optimized with CrystalPlan software[14] were used to ensure better than 95% coverage of a hemisphere of reciprocal space. Each orientation was measured for approximately 3 h. Raw peaks intensities were obtained using the 3-D ellipsoidal Q-space integration method available in Mantid.[15] Data normalization, including Lorentz, neutron 6 TOF spectrum, and detector efficiency corrections, were carried out with the ANVRED3 program.[16] A Gaussian numerical absorption correction was applied with $\mu = 1.1237 + 0.8375\ \lambda\ cm^{-1}$. The reduced data were saved in SHELX HKLF2 format, in which the neutron wavelength for each reflection was recorded separately. Non-hydrogen atom positions in the X-ray structure were used for the initial refinement of the neutron structure. Hydrogen atoms on carbon atoms are placed using the riding model available in SHELXL-2014.[17] The two hydrides of **2$_N$** were located from the difference Fourier map calculated using the neutron data. All atoms, including H, were refined anisotropically, and the neutron structure was then refined successfully to convergence using the SHELXL-2014 program. Selected distances and crystal data are listed in Tables 1 and S6. The structure reported herein has been deposited at the Cambridge Crystallographic Data Centre, CCDC no. 2095377.

Measurement Quantum Yield

The quantum yield of **3** is determined by a comparative method. Absolute values calculated by using $[Ru(bpy)_3]^{2+}$ as the standard sample according to the following equation:

$$\Phi_a = \frac{\frac{F_a}{A_a} x\, \eta_a^2}{\frac{F_s}{A_s} x \eta_s^2} x \Phi_s$$

The subscripts "s" and "a" denote standard and analyte, respectively, Φ is the fluorescence quantum yield, F is the integrated fluorescence intensity, A is the absorbance, and η is the refractive index of the solvent. The standard sample and compound **3** were measured two times, respectively. The experimental parameters are listed in the following table.

	Solvent	Absorbance (A)	Integrated fluorescence intensity (F)	F/A (*10^8)	Avg. F/A (*10^8)	Quantum Yield (Φ)
Standard	H_2O	0.101	6.14E+07	6.08	4.38	0.040[18]
Standard	H_2O	0.136	9.03E+07	6.64		
3	2-MeTHF	0.136	6.42E+07	4.72	1.35	0.033
3	2-MeTHF	0.141	6.84E+07	4.86		

Computational Detail

Geometry optimizations were performed by DFT calculations with the Gaussian 16 package, [19] using the PBE0 functional, [20] and the all-electron Def2-TZVP set from EMSL Basis Set Exchange Library.[21] All the optimized geometries were characterized as true minima on their potential energy surface by harmonic vibrational analysis. The Wiberg bond indices were computed with the NBO 6.0 program. [22] The UV-visible transitions were calculated by means of TD-DFT calculations.[23] Only singlet-singlet, *i.e.* spin-allowed, transitions were computed. The UV–visible spectra were simulated from the computed from the TD-DFT transitions and their oscillator strengths by using the SWizard program,[24] each transition being associated with a Gaussian function of half-height width equal to 3000 cm^{-1}. The compositions of the molecular orbitals were calculated using the AOMix program.[25] The ^1H chemical shifts were computed according to the gauge including atomic orbital (GIAO).[26]

References

1. R. P. B. Silalahi, G. -R. Huang, J. -H. Liao, T. -Z. Chiu, K. K. Chakrahari, X. Wang, J. Cartron, S. Kahlal, J. -Y. Saillard, C. W. Liu, *Inorg. Chem*. **2020**. *59*. 2536–2547.
2. G. J. Kubas, *Inorg. Synth.* **1979**, *19*, 90-92.
3. A. A. M. Aly, B. Walfort, H. Lang, *Kristallogr. NCS.* **2004**, *219*, 489-491.
4. J. L. Burmeister, N. DeStefano, *Inorg. Chem*. **1971**, *10*, 998-1003.
5. P. Wystrach, E. O. Hook, G. L. M. Christopher, *J. Org. Chem*. **1956**, *21*, 705−707.
6. a) R. S. Dhayal, J. -H. Liao, X. Wang, Y. -C. Liu, M. -H. Chiang, S. Kahlal, J. -Y. Saillard, C. W. Liu, *Angew. Chem. Int. Ed.* **2015**, *54*, 13604-13608. *Angew. Chem*, **127**, 13808-13812; b) R. S. Dhayal, J. -H. Liao, Y. -R. Lin, P. -K. Liao, S. Kahlal, J. -Y. Saillard, C. W. Liu, *J. Am. Chem. Soc.* **2013**, *135*, 4704-4707.
7. R. P. B. Silalahi, T. -H, Chiu, J. -H. Kao, C. -Y. Wu, C. -W. Yin, Y. -C. Liu, Y. J. Chen. J. -Y. Saillard, M. -H. Chiang, C. W. Liu, *Inorg. Chem*. **2021**, *60*, 10799-10807.
8. G. M. Sheldrick, SADABS, version 2014-11.0, Bruker Area Detector Absorption Corrections; Bruker AXS Inc.: Madison, WI, **2014**.
9. G. M. Sheldrick, v4.043, Software for the CCD Detector System; Siemens Analytical Instruments: Madison, WI, 1995.
10. G. M. Sheldrick. *Acta Crystallogr., Sect. A: Found. Crystallogr.* **2008**, *A64*, 112– 122, DOI: 10.1107/S0108767307043930
11. T. Gruene, H. W. Hahn, A. V. Luebben, F. Meilleur, G. M. Sheldrick, *J. Appl. Crystallogr.* **2014**, *47*, 462– 466, DOI: 10.1107/S1600576713027659
12. G. M. Sheldrick, G. M. SHELXL, version 6.14 (PC version) Program Library for Structure Solution and Molecular Graphics, Bruker Analytical X-ray Systems, Madison, Wisconsin, USA, **2003**.
13. Z. L. Xue, A. J. Ramirez-Cuesta, C. M. Brown, S. Calder, H. B. Cao, B. C. Chakoumakos, L. L. Daemen, A. Huq, A. I. Kolesnikov, E. Mamontov, A. A. Podlesnyak, X. P. Wang, *Eur. J. Inorg. Chem.* **2019**, *8*, 1065–1089.
14. J. Zikovsky, P. Peterson, X. Wang, M. Frost, C. Hoffmann, *J. Appl. Crystallogr.* **2011**, *44*, 418–423.
15. A. J. Schultz, M. Jorgensen, X. Wang, R. Mikkelson, D. Mikkelson, V. Lynch, P. Peterson, M. Green, C. Hoffmann, *J. Appl. Crystallogr.* **2014**, *47*, 915–921.
16. A. J. Schultz, K. Srinivasan, R. G. Teller, J. M. Williams, C. M. Lukehart, *J. Am. Chem. Soc.* **1984**, *106*, 999–1003.
17. G. M. Sheldrick, *Acta Crystallogr. Sect. C: Struct. Chem.* **2015**, *C71*, 38.

18. K. Suzuki, A. Kobayashi, S. Kaneko, K. Takehira, T. Yoshihara, H. Ishida, Y. Shiina, S. Oishi, S. Tobita, S, *Phys. Chem. Chem. Phys*. **2009**, *11*, 9850-9860.
19. Gaussian 16, Revision C.01, M. J. Frisch, G. W. Trucks, H. B. Schlegel, G. E. Scuseria, M. A. Robb, J. R. Cheeseman, G. Scalmani, V. Barone, G. A. Petersson, H. Nakatsuji, X. Li, M. Caricato, A. V. Marenich, J. Bloino, B. G. Janesko, R. Gomperts, B. Mennucci, H. P. Hratchian, J. V. Ortiz, A. F. Izmaylov, J. L. Sonnenberg, D. Williams-Young, F. Ding, F. Lipparini, F. Egidi, J. Goings, B. Peng, A. Petrone, T. Henderson, D. Ranasinghe, V. G. Zakrzewski, J. Gao, N. Rega, G. Zheng, W. Liang, M. Hada, M. Ehara, K. Toyota, R. Fukuda, J. Hasegawa, M. Ishida, T. Nakajima, Y. Honda, O. Kitao, H. Nakai, T. Vreven, K. Throssell, J. A. Montgomery, Jr., J. E. Peralta, F. Ogliaro, M. J. Bearpark, J. J. Heyd, E. N. Brothers, K. N. Kudin, V. N. Staroverov, T. A. Keith, R. Kobayashi, J. Normand, K. Raghavachari, A. P. Rendell, J. C. Burant, S. S. Iyengar, J. Tomasi, M. Cossi, J. M. Millam, M. Klene, C. Adamo, R. Cammi, J. W. Ochterski, R. L. Martin, K. Morokuma, O. Farkas, J. B. Foresman, and D. J. Fox, Gaussian, Inc., Wallingford CT, 2016.
20. C. Adamo, V. Barone, *J. Chem. Phys.* **1999**, *110*, 6158-6169.
21. F. Weigend, R. Ahlrichs, *Phys. Chem. Chem. Phys.* **2005**, *7*, 3297-32305.
22. E. D. Glendening, J. K. Badenhoop, A. E. Reed, J. E. Carpenter, J. A. Bohmann, C. M. Morales, C. R. Landis, F. Weinhold, F. NBO 6.0; Theoretical Chemistry Institute, University of Wisconsin, Madison, WI, 2013, http://nbo6.chem.wisc.edu.
23. C. Ullrich, C. Time-Dependent Density-Functional Theory, Concepts and Applications, Oxford University Press, NewYork, 2012.
24. S. I. Gorelsky, SWizard program, revision 4.5, http://www.sg-chem.net.
25. S. I. Gorelsky, AOMix program, http://www.sg-chem.net.
26. a) F. London, *J. Phys. Radium* **1937**, *8*, 397-409; b) R. McWeeny, *Phys. Rev*. **1962**, *126*, 1028–1034; c) R. Ditchfield, *Mol. Phys*. **1974**, *27*, 789-807; d) J. L. Dodds, R. McWeeny, A. J. Sadlej, *Mol. Phys*. **1977**, *34*, 1779-1791; e) K. Wolinski, J. F. Hinton, P. Pulay, *J. Am. Chem. Soc*. **1990**, *112*, 8251-8260.

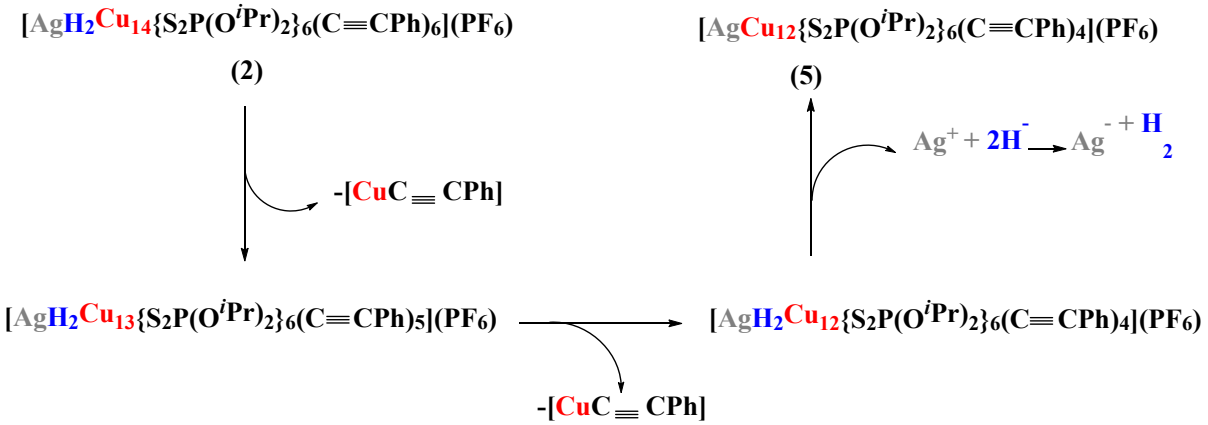

Scheme S1. Degradation of cluster **2** into a 2-electron bimetallic cluster **5** via successive losses of [CuCCPh] followed by an internal redox reaction.

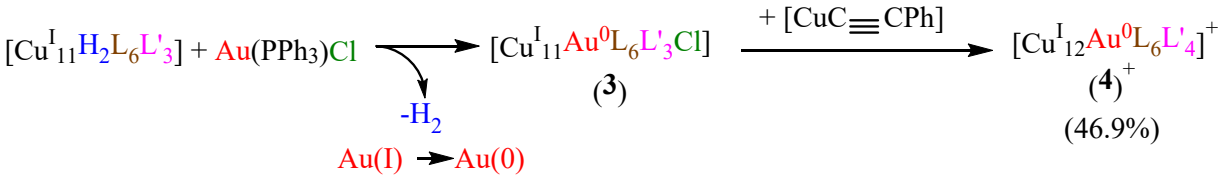

L = $[S_2P(O^iPr)_2]$
L'= C≡CPh

Scheme S2. Formation of compound **4** from **3** via reacting with one equiv. of [CuC≡CPh]. The 2-e superatomic alloy **3** is formed via an internal redox reactions.

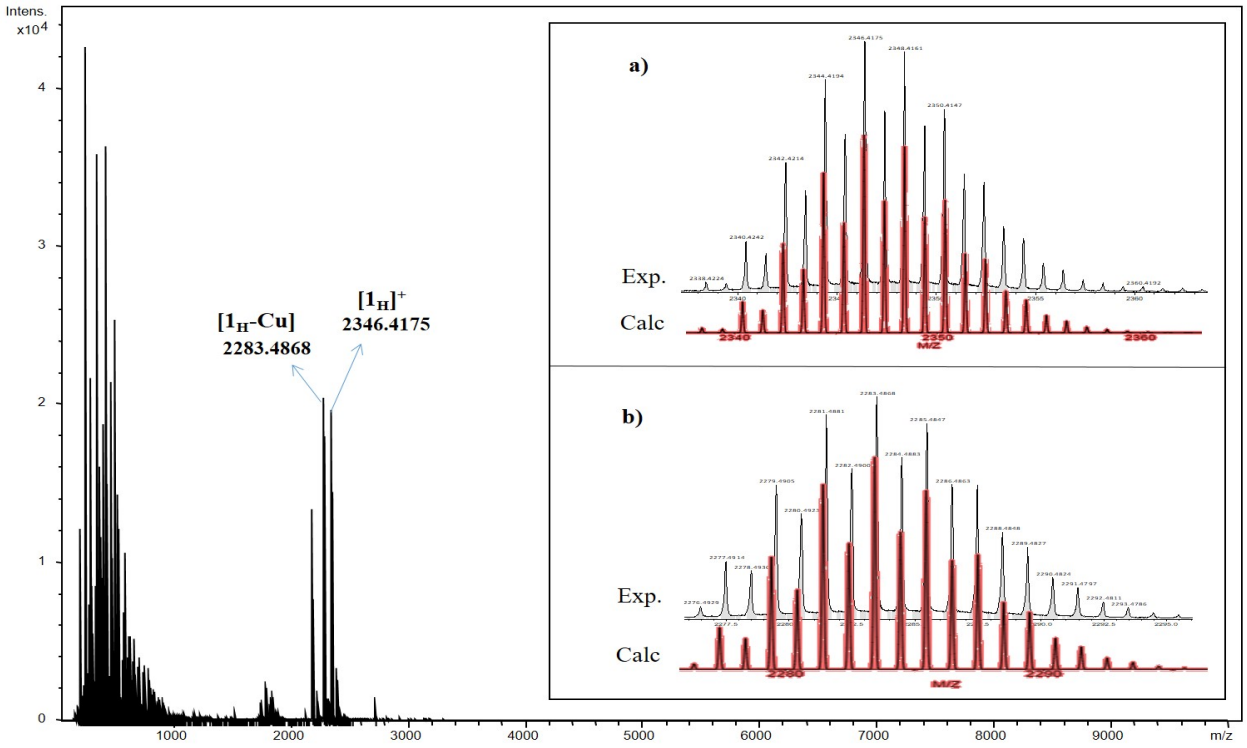

Figure S1. ESI-MS spectra of cluster $[\mathbf{1_H}]^+$ and $[\mathbf{H_2Cu_{11}}]$ in positive mode. Inset: Experimental one in top (black) and theoretical one in bottom (red) of (a) $[\mathbf{1_H}]^+$ and (b) $[\mathbf{H_2Cu_{11}}]$.

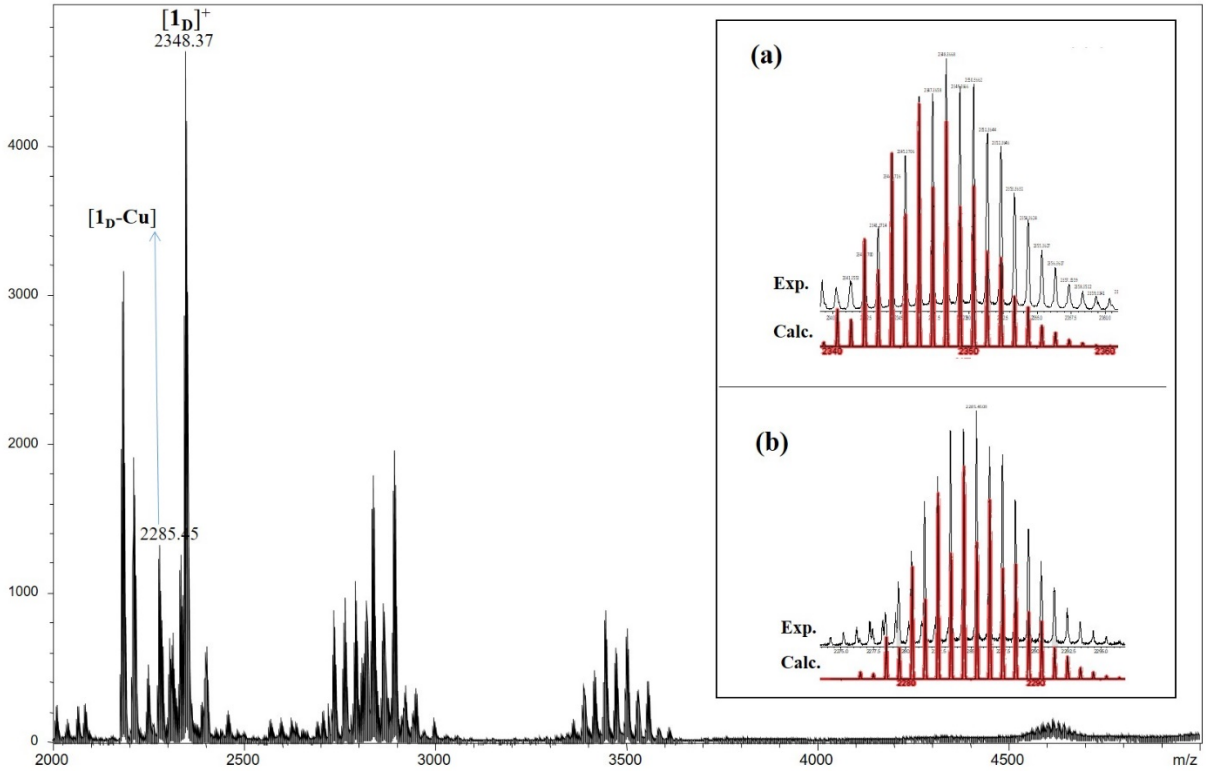

Figure S2. ESI-MS spectra of cluster $[\mathbf{1_D}]^+$ and $[\mathbf{D_2Cu_{11}}]$ in positive mode. Inset: Experimental one in top (black) and theoretical one in bottom (red) of (a) $[\mathbf{1_D}]^+$ and (b) $[\mathbf{D_2Cu_{11}}]$.

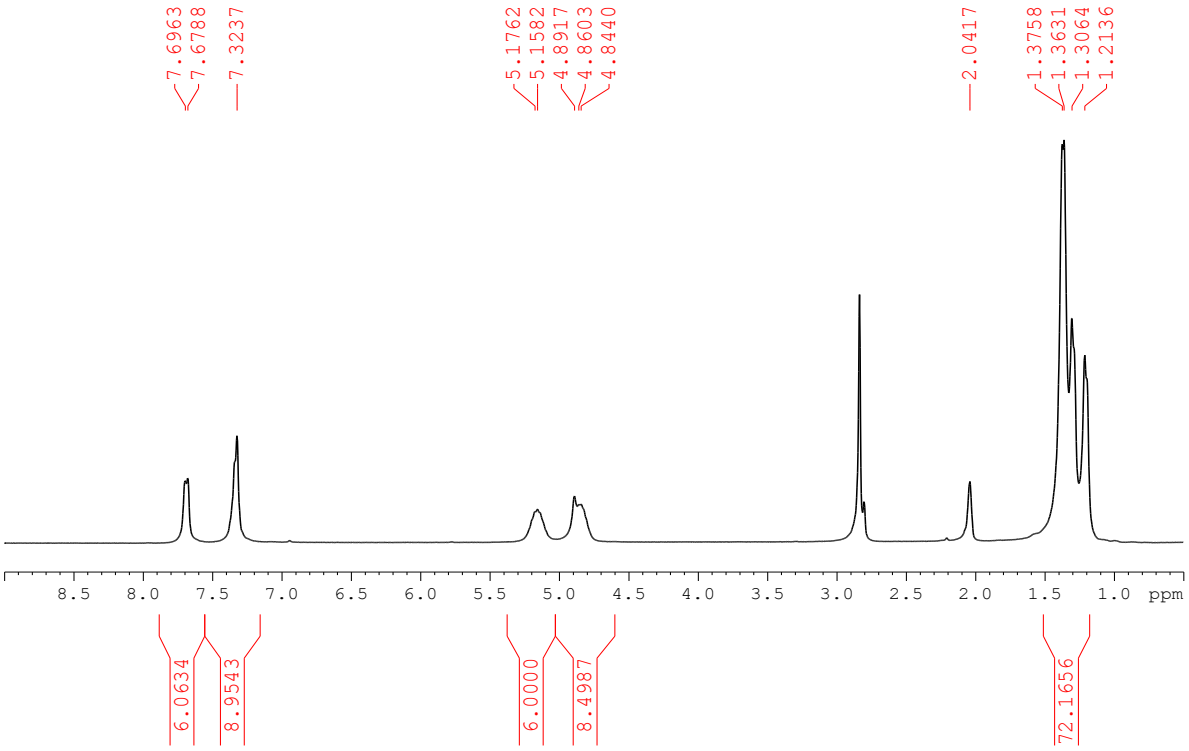

Figure S3. ^{1}H NMR spectrum of compound $[Cu_{11}H_2\{S_2P(O^iPr)_2\}_6(C{\equiv}CPh)_3]$ (**H_2Cu_{11}**) in *d_6*-acetone.

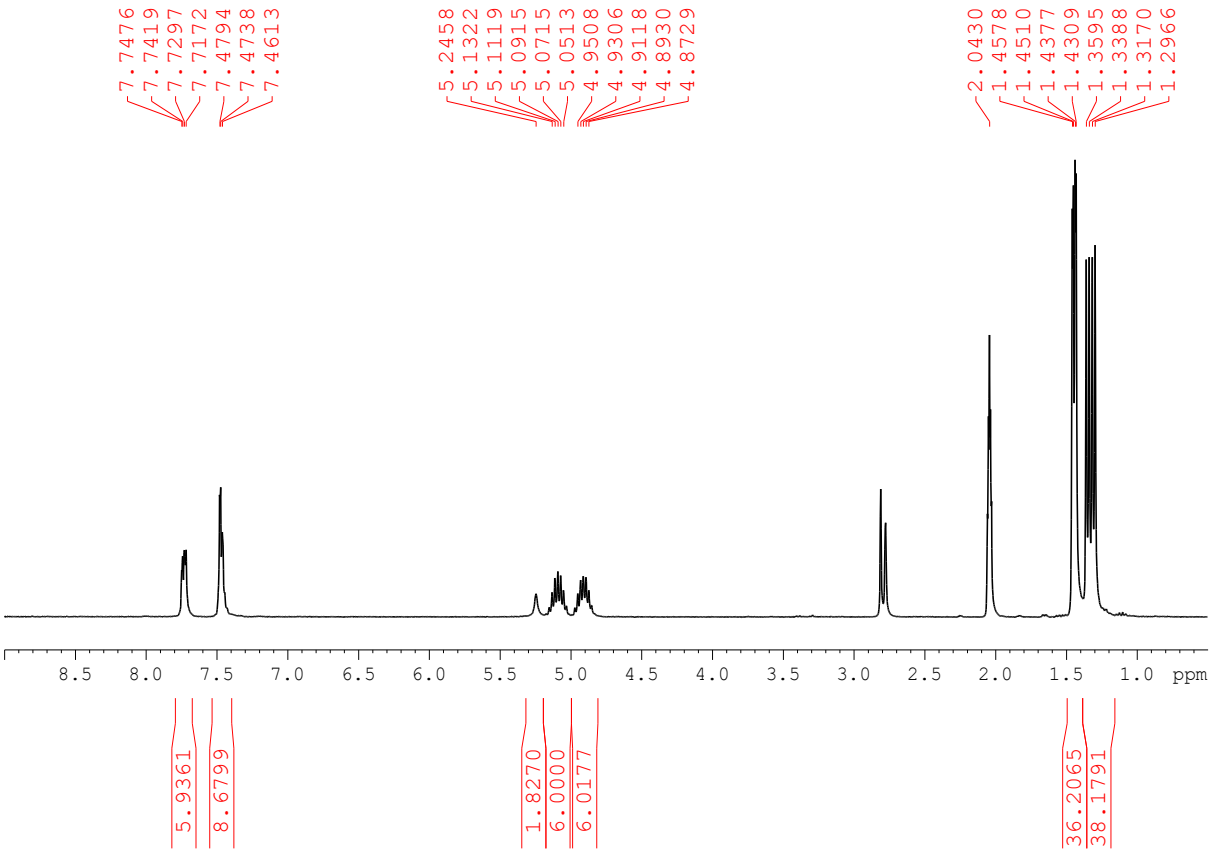

Figure S4. ^{1}H NMR spectrum of cluster **1_H** in *d_6*-acetone.

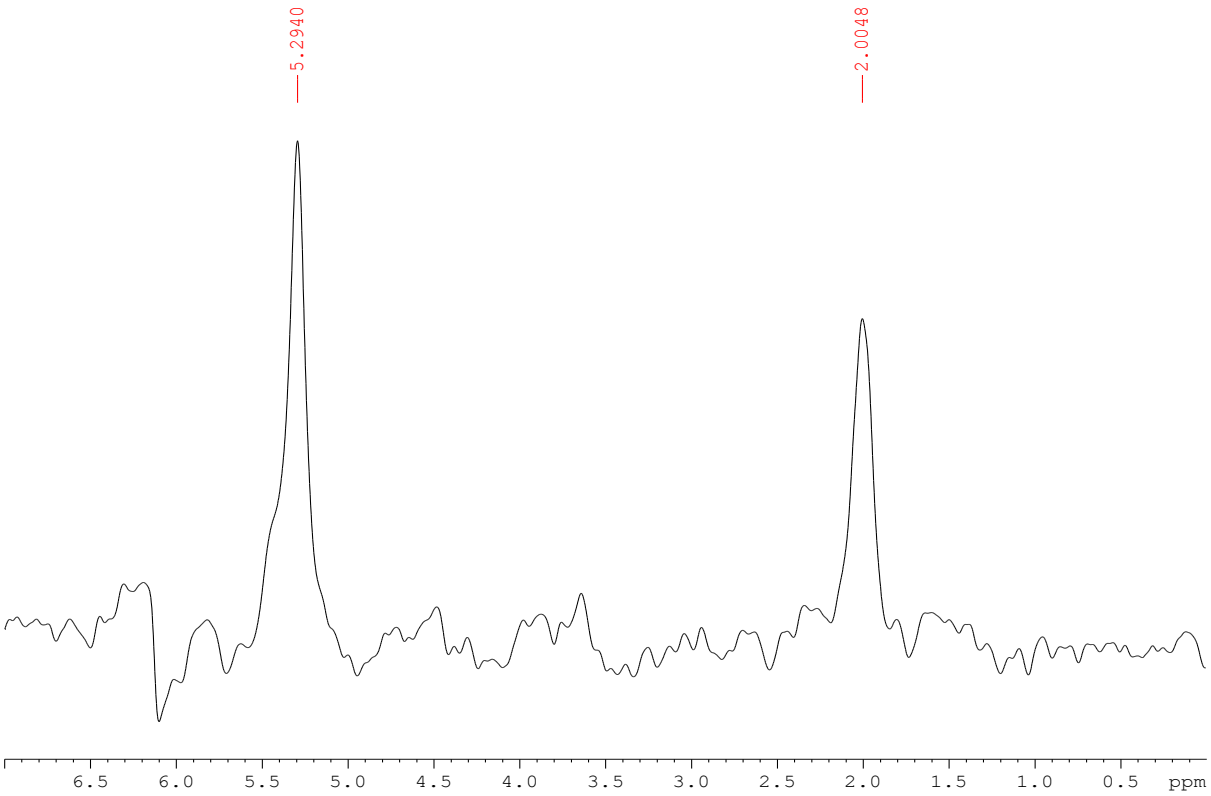

Figure S5. ^{2}H NMR spectrum of compound $\mathbf{1_D}$ in acetone solvent.

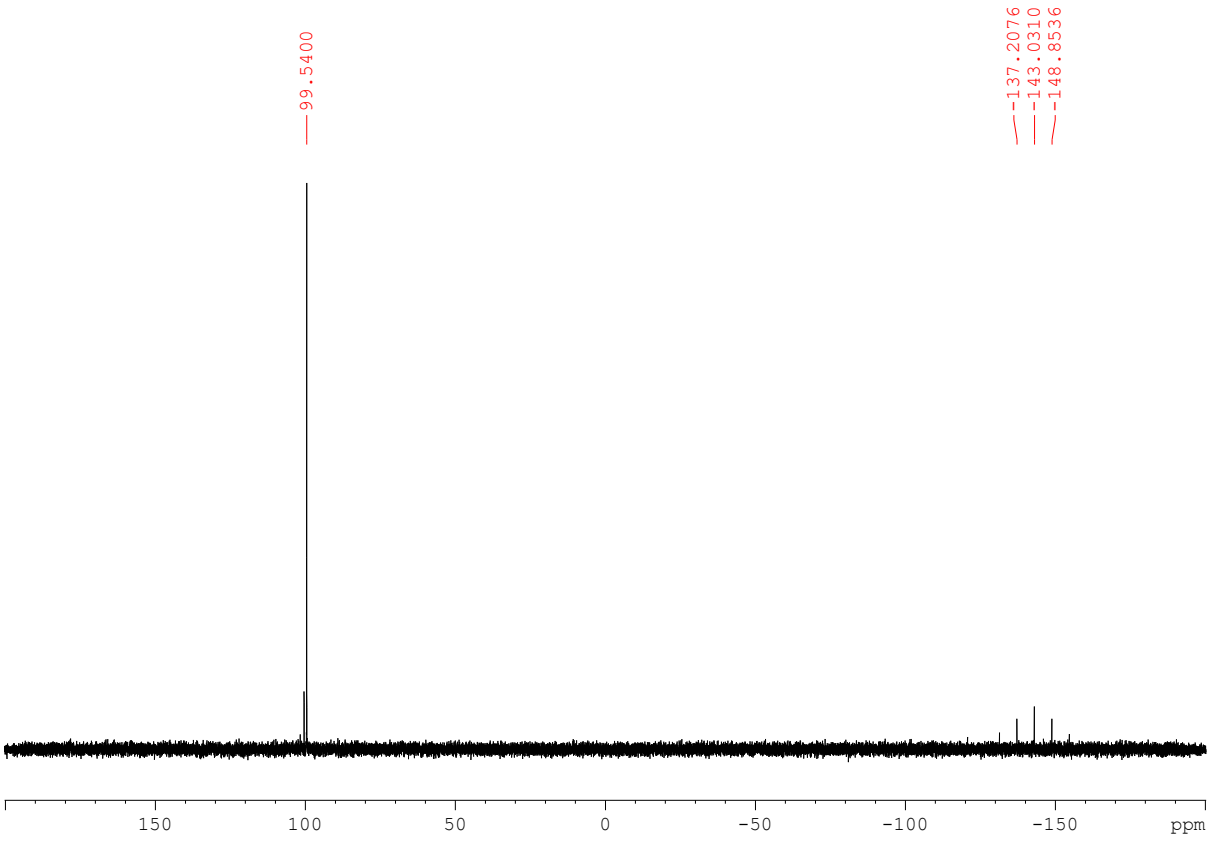

Figure S61. ^{31}P $\{^{1}$H$\}$ NMR spectrum of compound $\mathbf{1_H}$ in d_6-acetone.

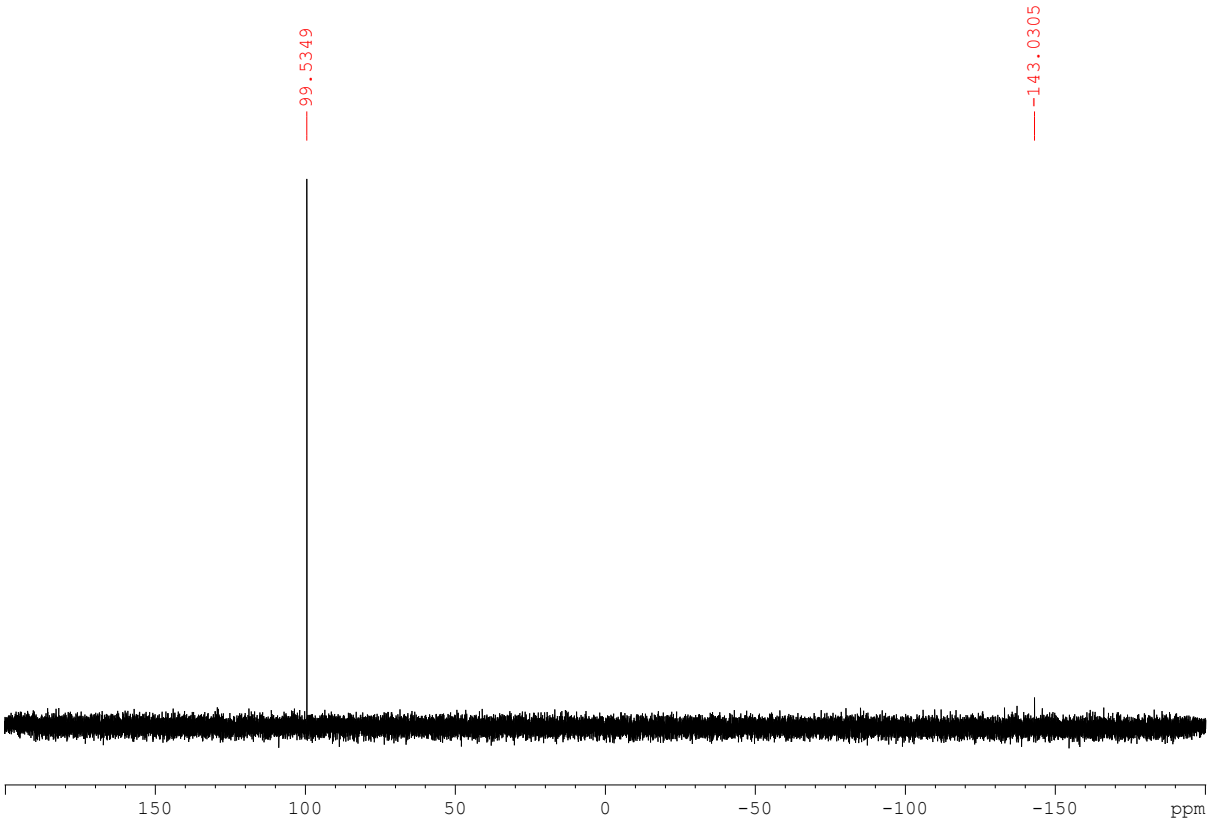

Figure S7. ^{31}P $\{^{1}H\}$ NMR spectrum of cluster **1D** in d_6-acetone.

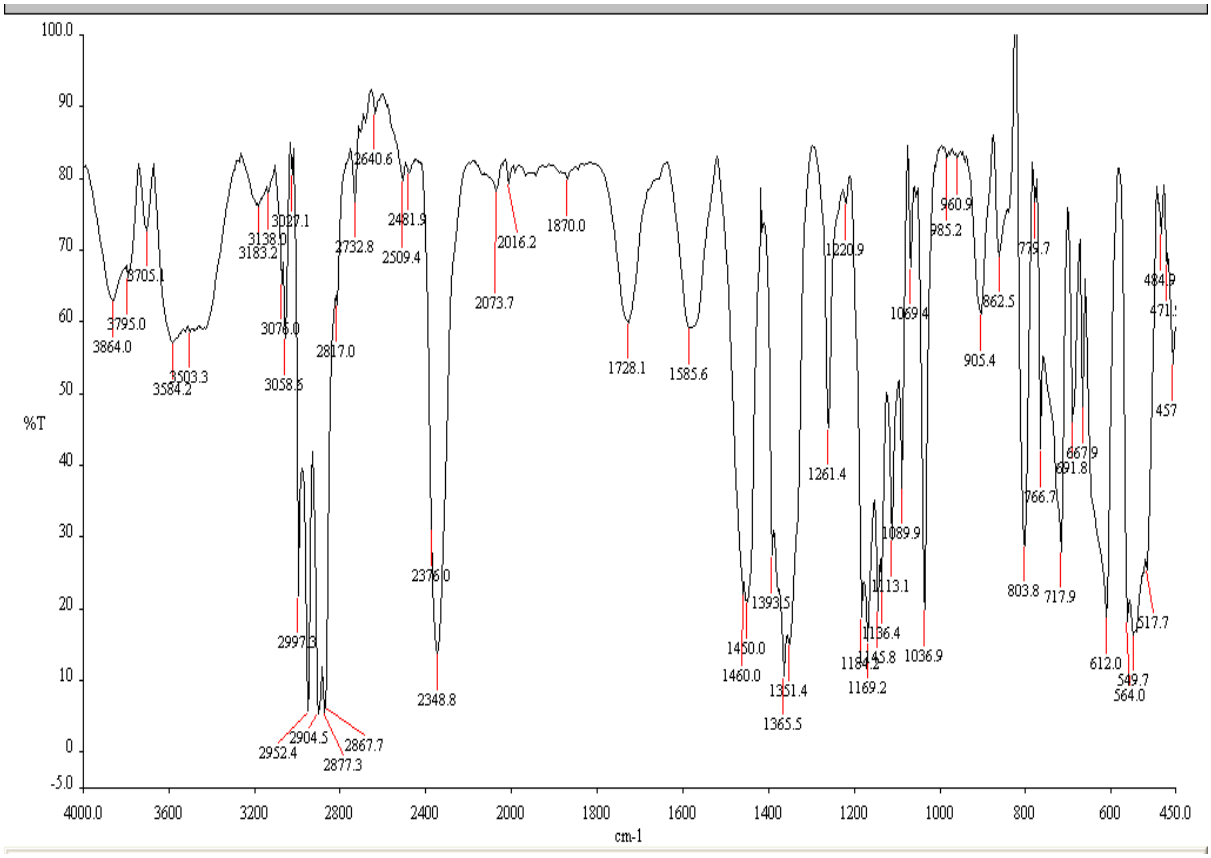

Figure S8. FT-IR spectra of cluster **1H**.

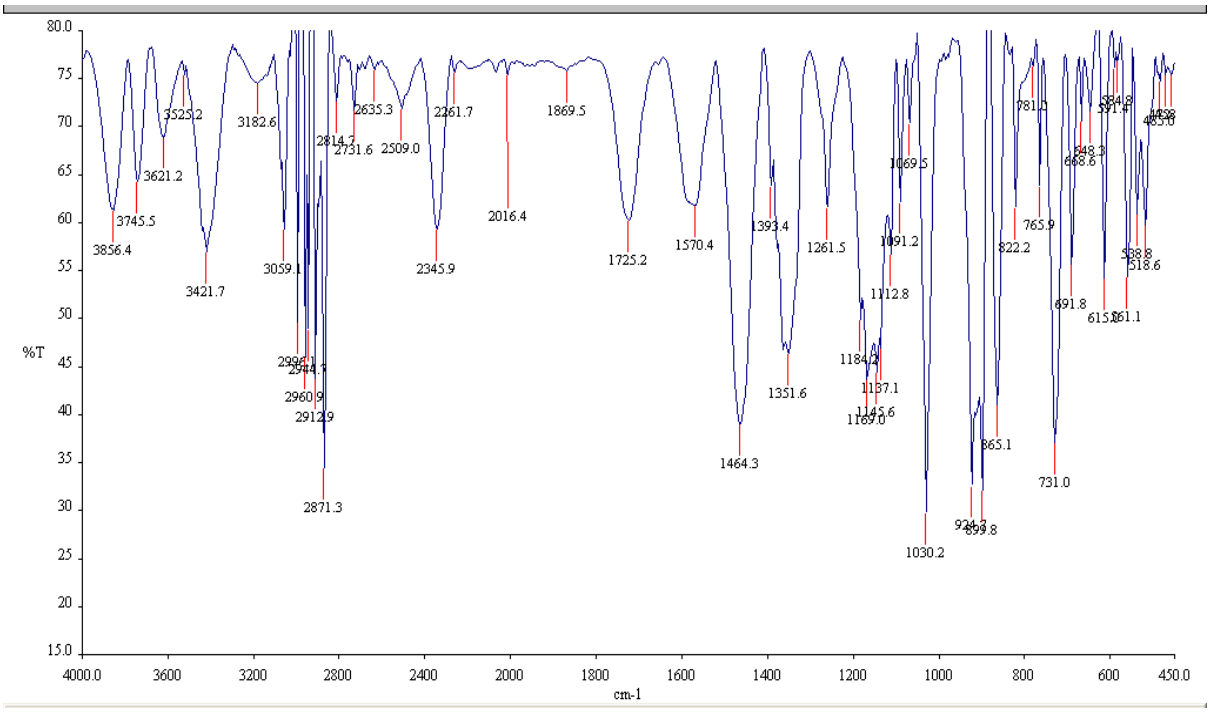

Figure S9. FT-IR spectra of cluster **1D**.

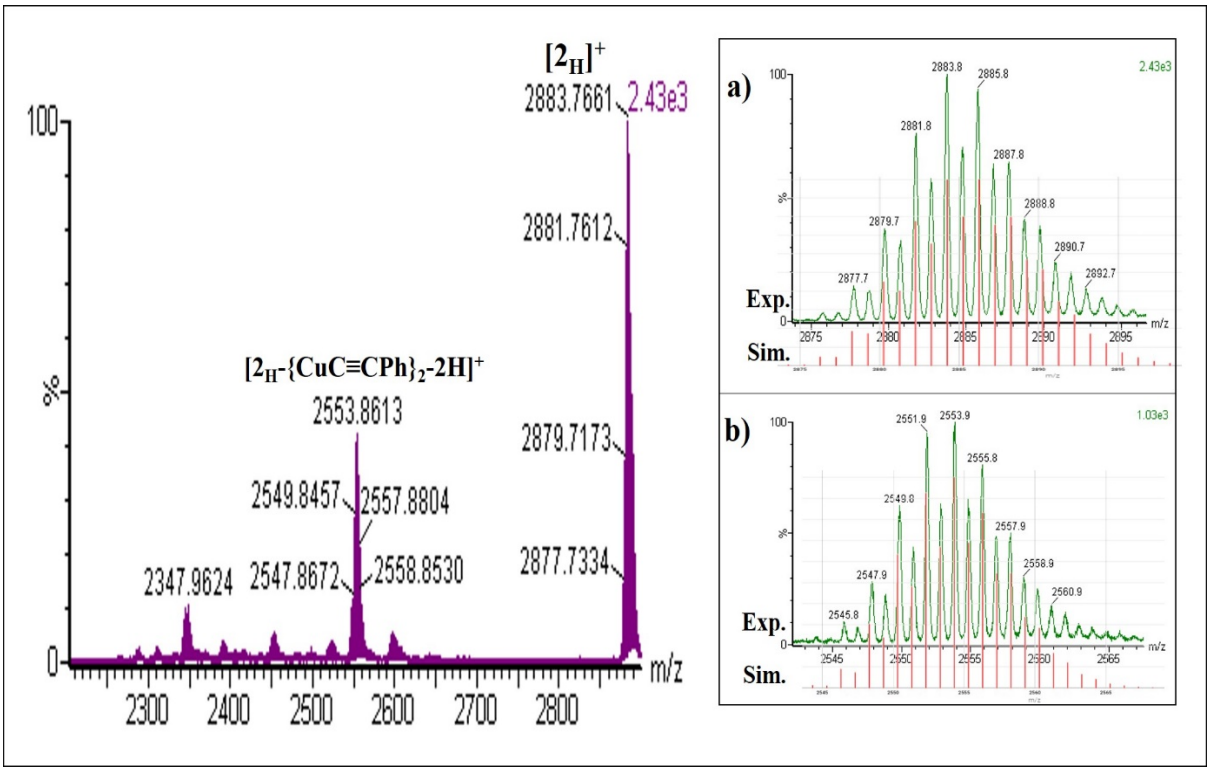

Figure S10. ESI-MS spectra of cluster $[\mathbf{2_H}]^+$ and $[\mathbf{2_H}\text{-}\{\mathbf{CuC{\equiv}CPh}\}_2\text{-}\mathbf{2H}]^+$ in positive mode. Inset: Experimental one in top (green) and simulation one in bottom (red) of (a) $[\mathbf{2_H}]^+$ and (b) $[\mathbf{2_H}\text{-}\{\mathbf{CuC{\equiv}CPh}\}_2\text{-}\mathbf{2H}]^+$.

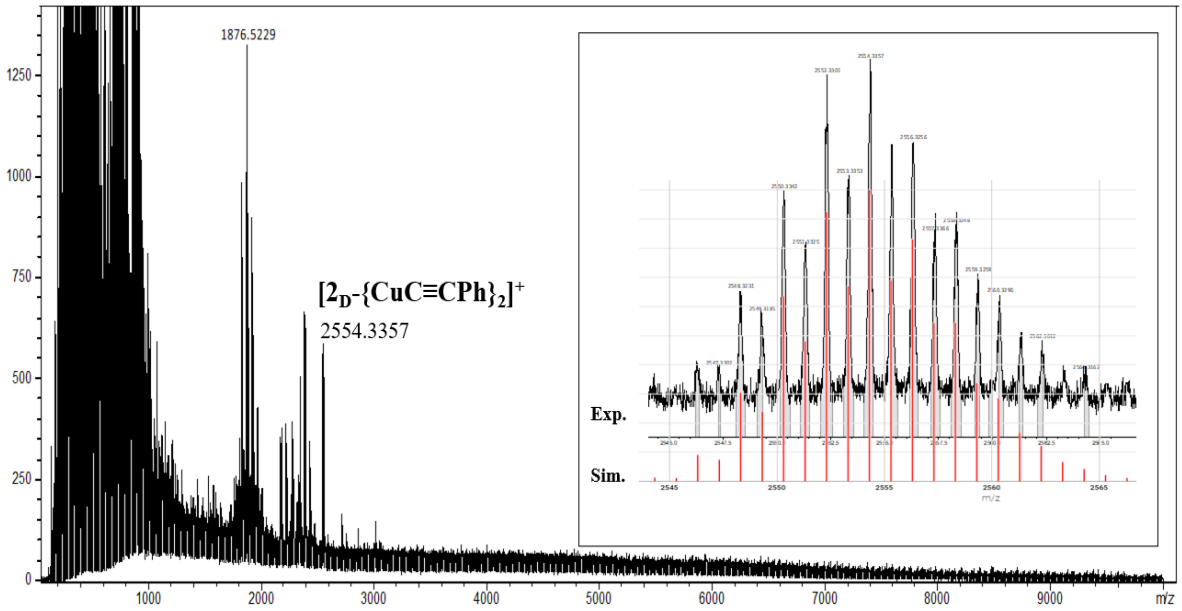

Figure S11. ESI-MS spectra of the cluster $[\mathbf{2_D\text{-}\{CuC{\equiv}CPh\}_2}]^+$ in positive mode. Inset: Experimental one in the top (black) and simulation one in the bottom (red) of $[\mathbf{2_D\text{-}\{CuC{\equiv}CPh\}_2}]^+$.

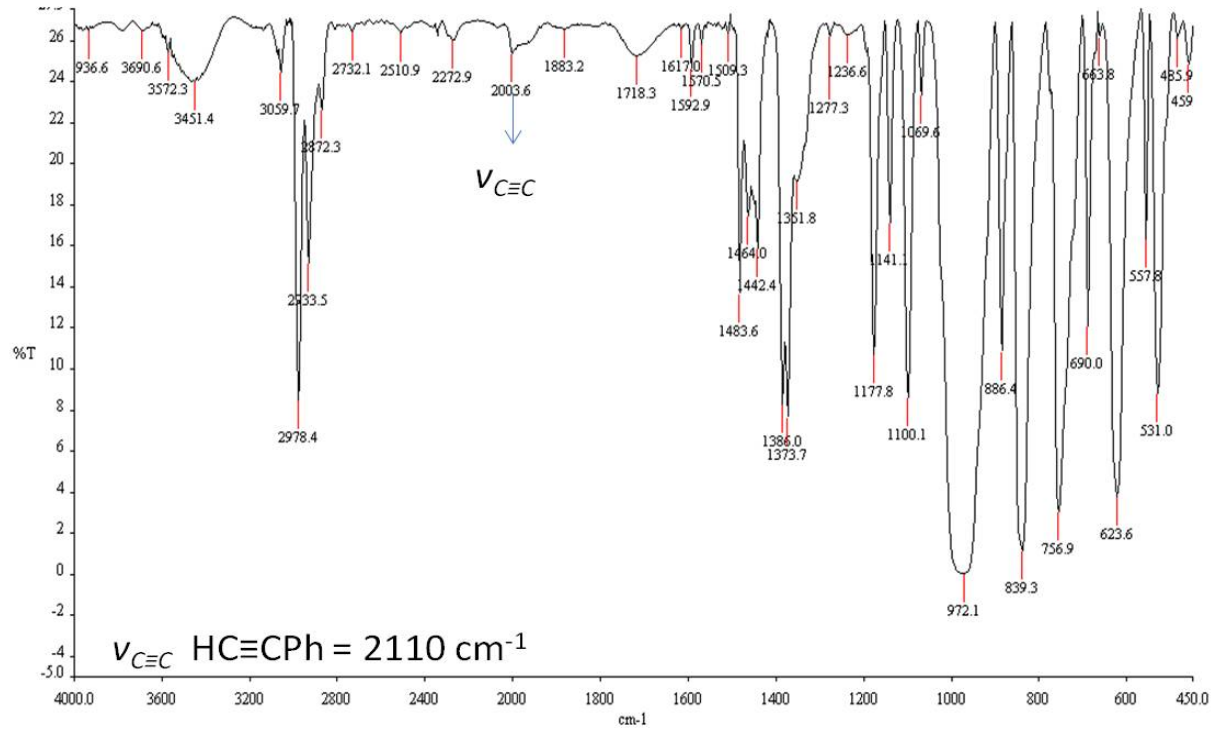

Figure S12. FT-IR spectra of cluster **2**.

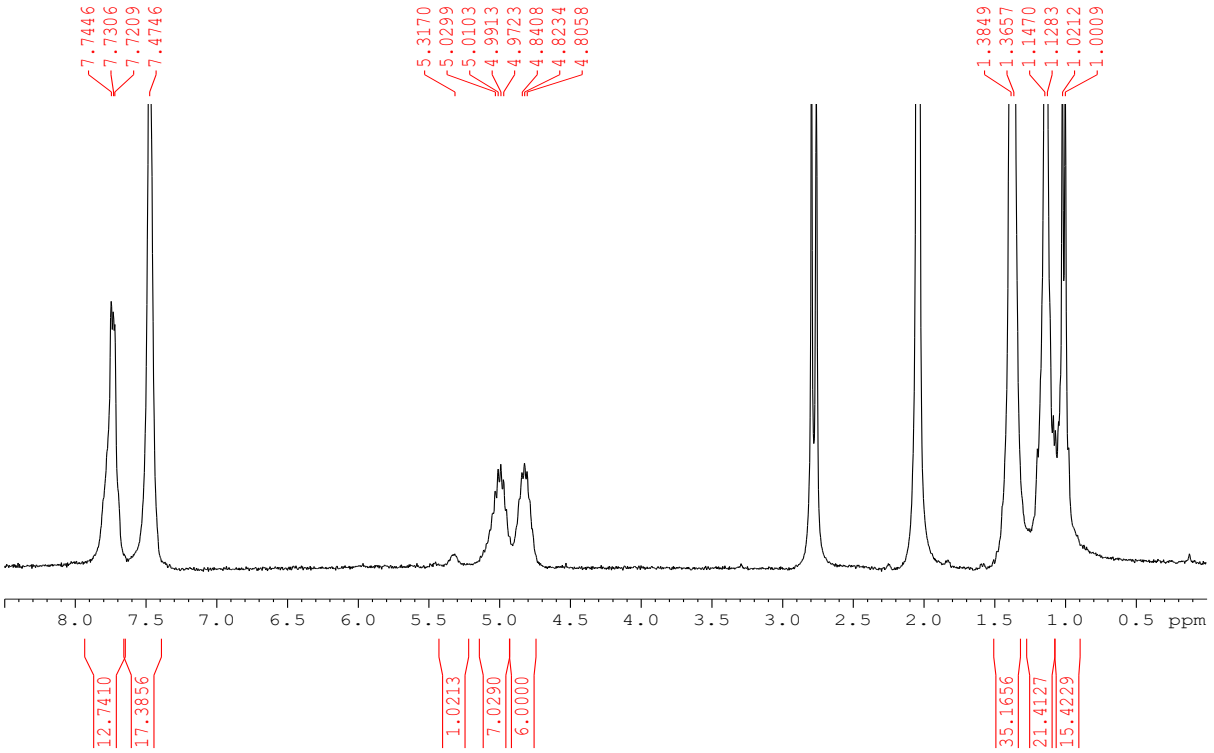

Figure S13. ^{1}H NMR spectrum of cluster $\mathbf{2_H}$ in d_6-acetone.

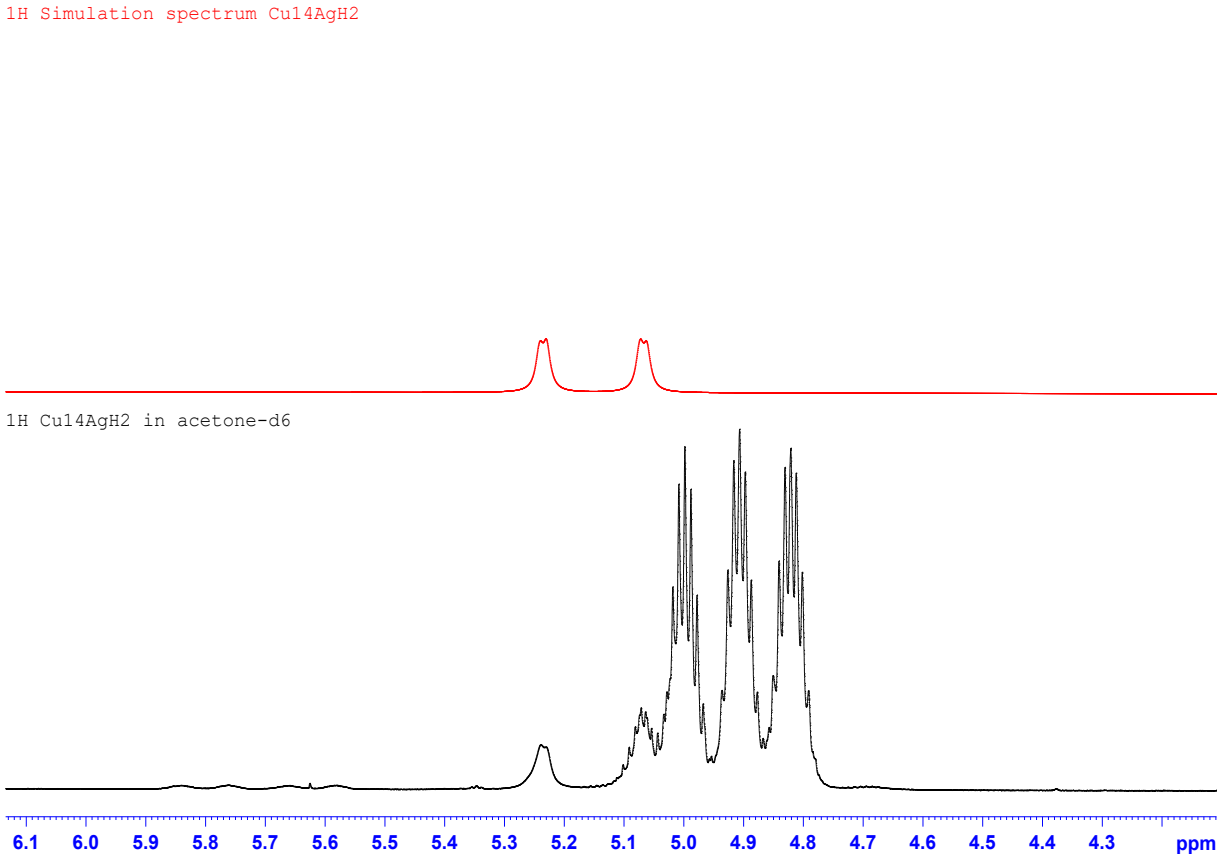

Figure S14. The simulated splitting pattern of hydrides (top) and ^{1}H NMR spectrum cluster **2** (bottom) at room temperature.

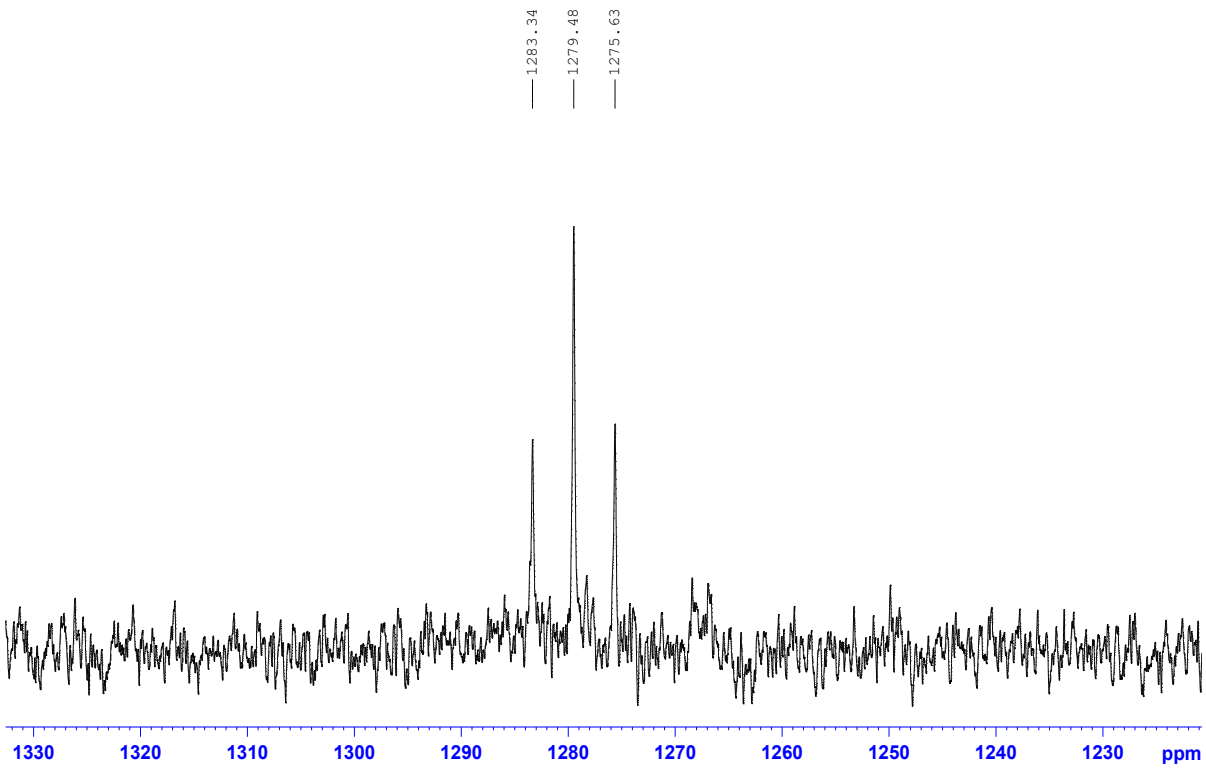

Figure S15. ^{109}Ag (27.918MHz, d_6-acetone) NMR spectrum cluster **2**.

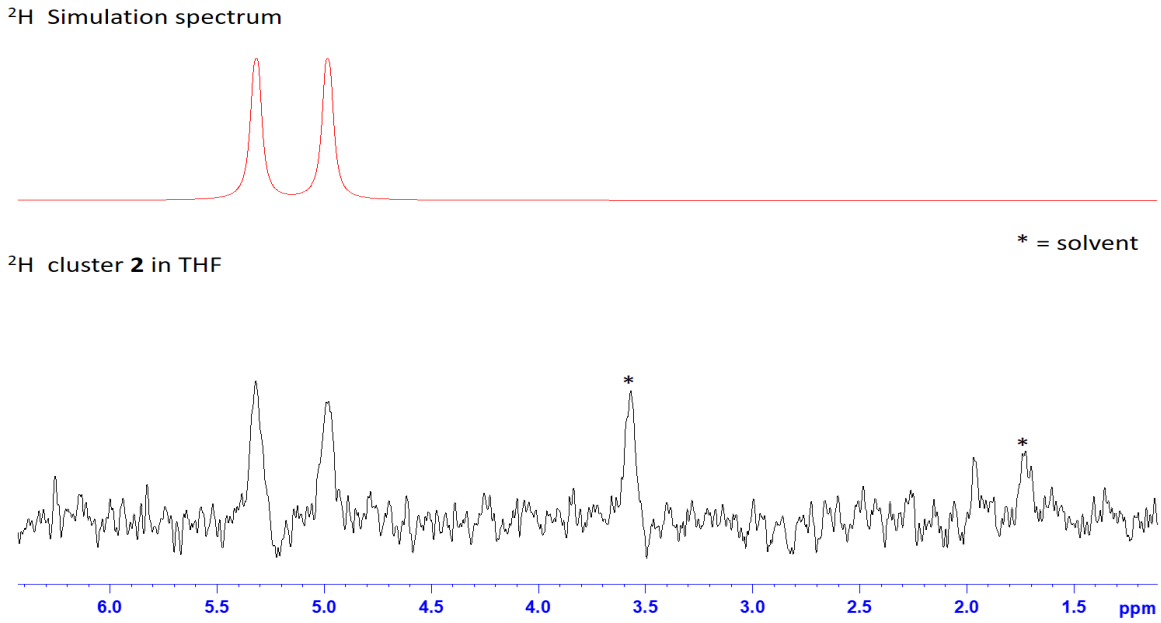

Figure S16. The simulated splitting pattern of deuteride (top) and ^{2}H NMR spectrum of cluster **2D** in tetrahydrofuran solvent (bottom) (46.1 MHz, room temperature).

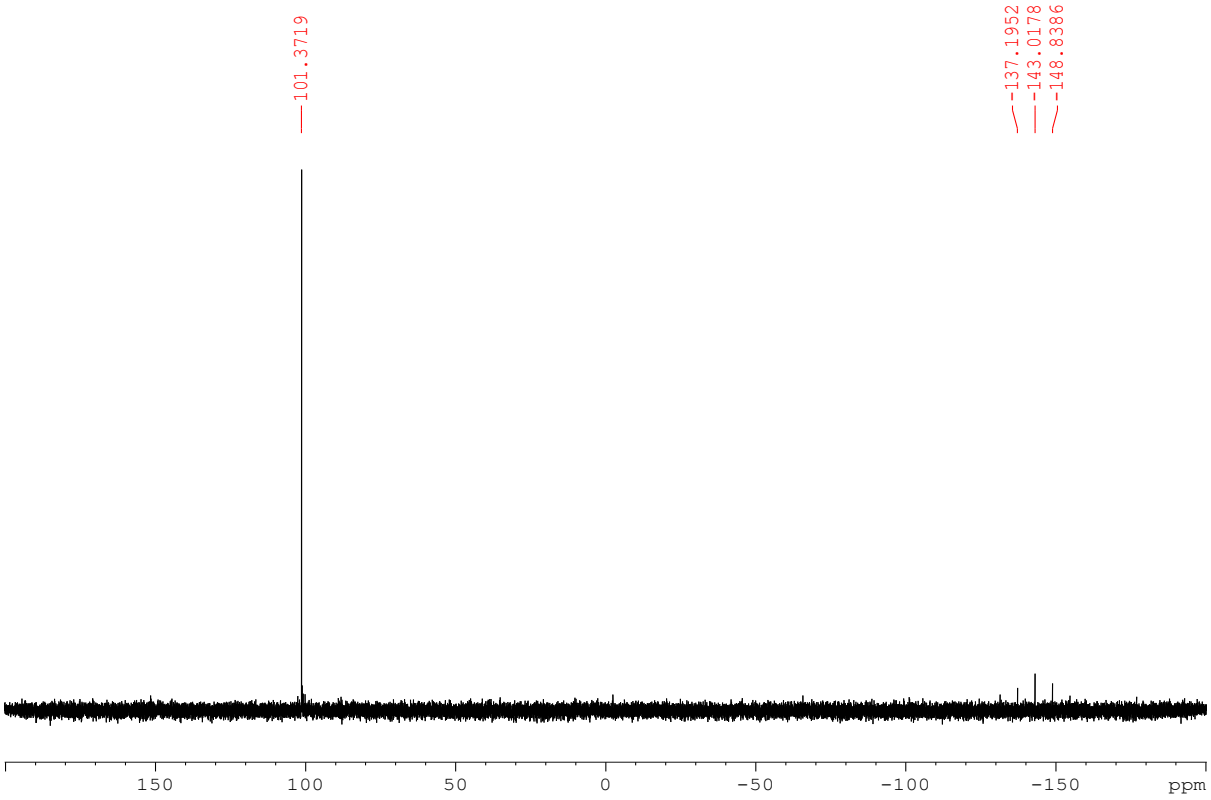

Figure S172. $^{31}P\{^{1}H\}$ NMR spectrum of compound **2H** in *d*6-acetone.

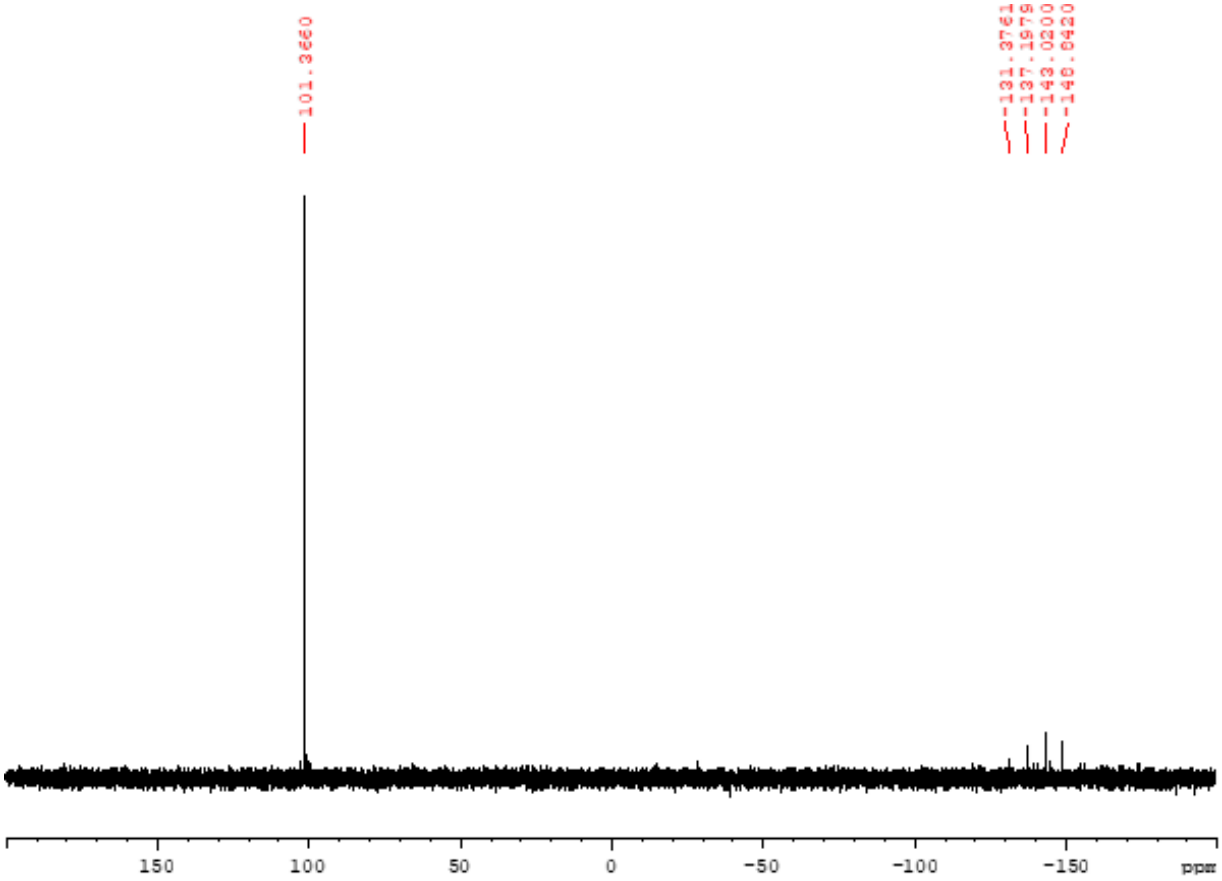

Figure S18. $^{31}P\{^{1}H\}$ NMR spectrum of compound **2D** in *d*6-acetone.

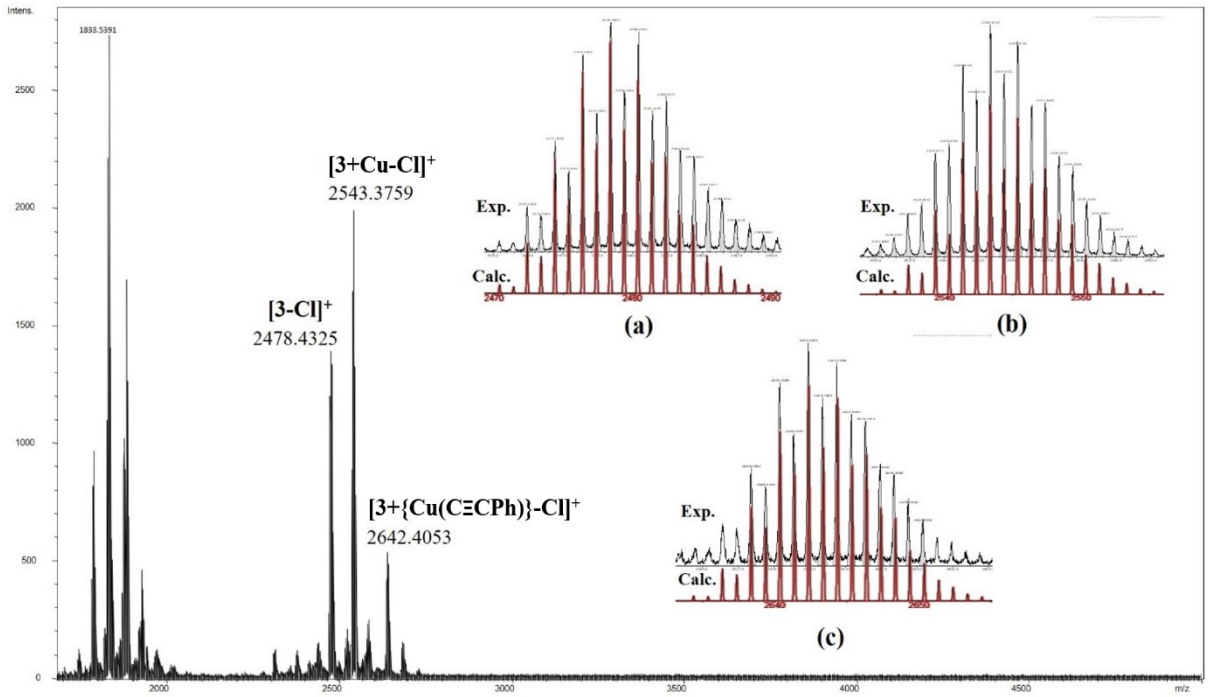

Figure S19. Positive-mode ESI-MS of [**3**-Cl]$^+$, [**3**+Cu-Cl]$^+$, and [**3**+(CuC≡CPh)-Cl]$^+$; inset show experimental (black) and simulated (red) isotopic distribution pattern (a) [**3**-Cl]$^+$, (b) [**3**+Cu-Cl]$^+$, and (c) [**3**+(CuC≡CPh)-Cl]$^+$.

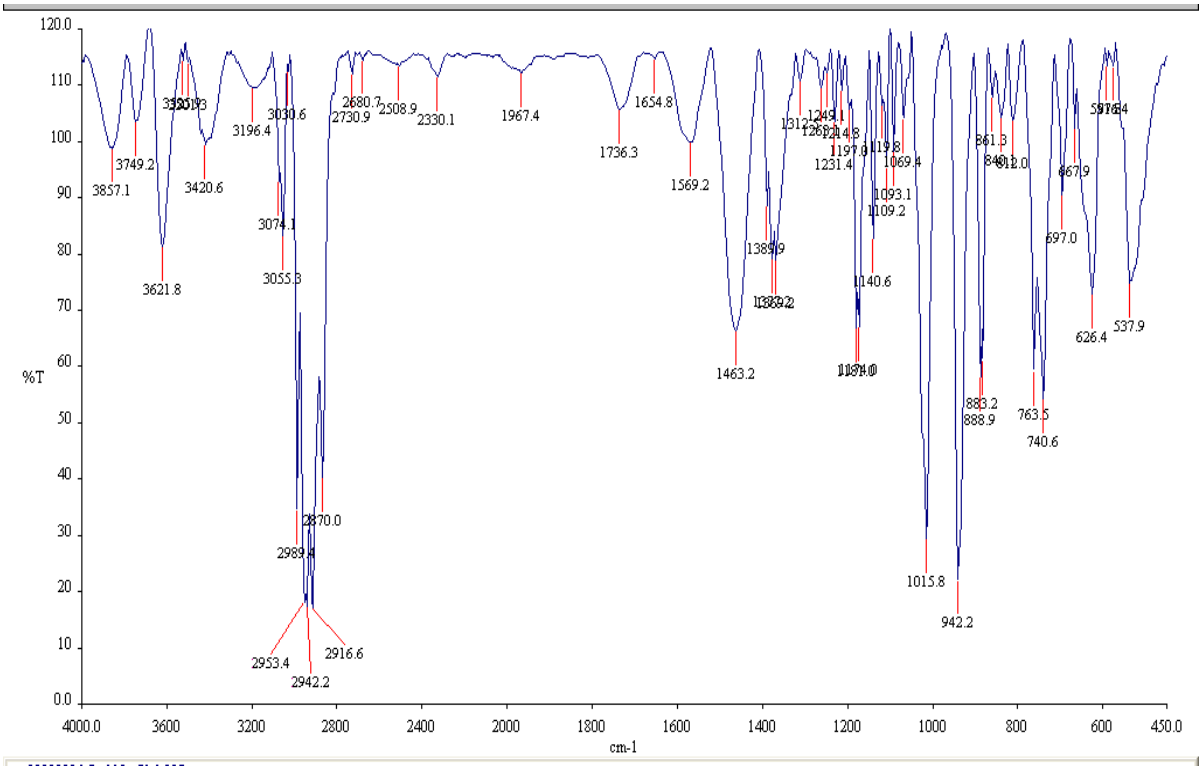

Figure S20. IR spectra of compound **3**.

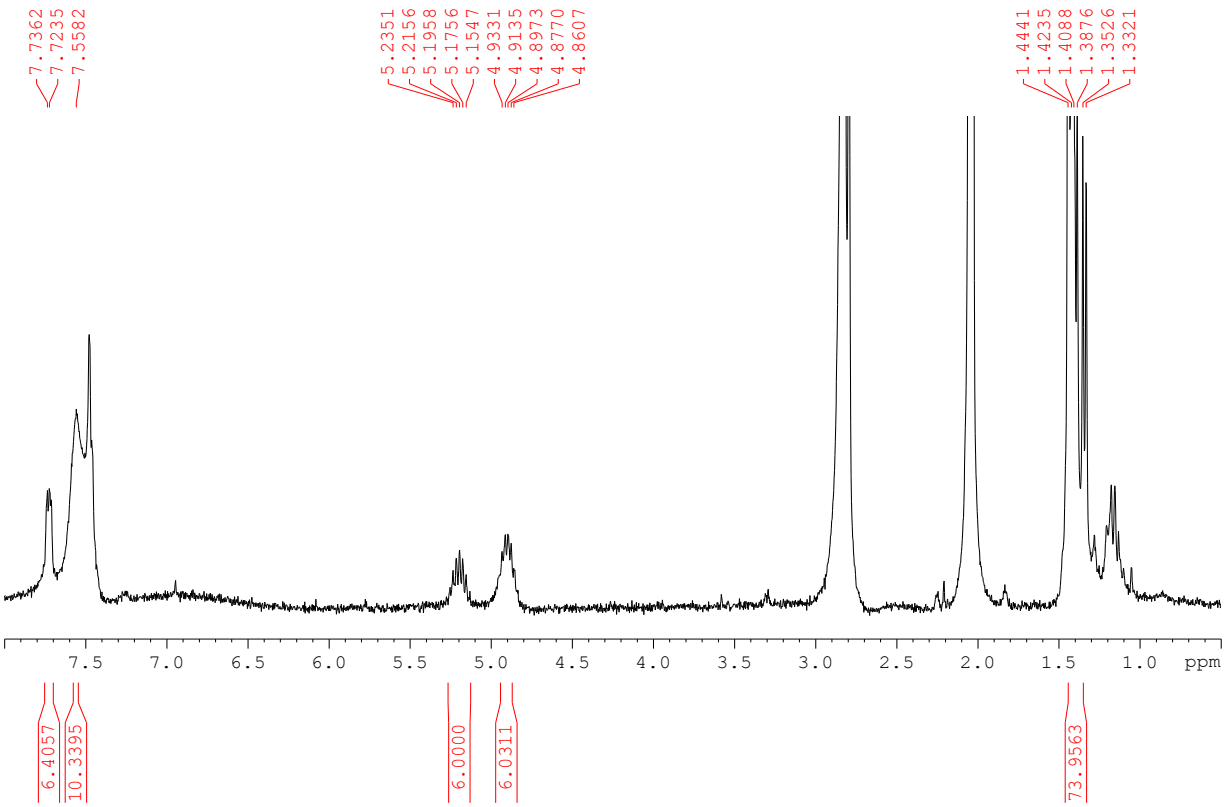

Figure S21. ^{1}H NMR spectrum of compound **3** in $CDCl_3$.

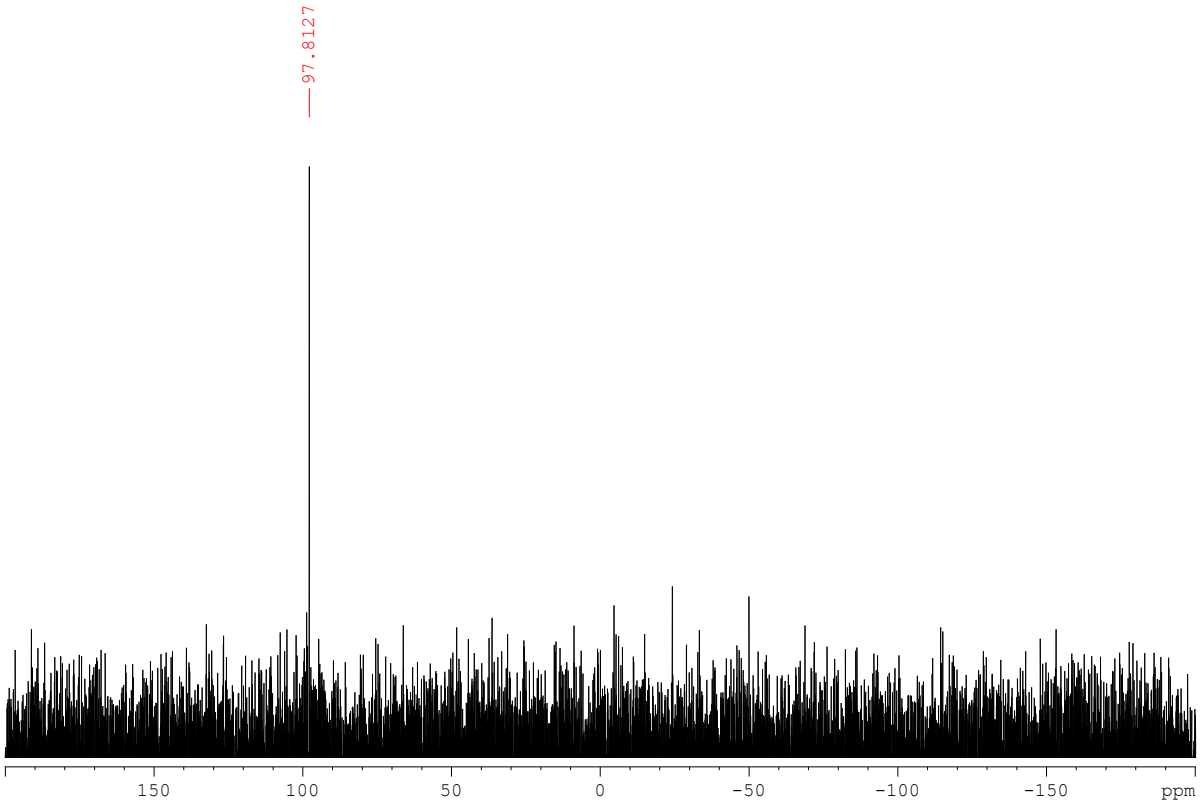

Figure S22. $^{31}P\{^{1}H\}$NMR spectrum of compound **3** in $CDCl_3$.

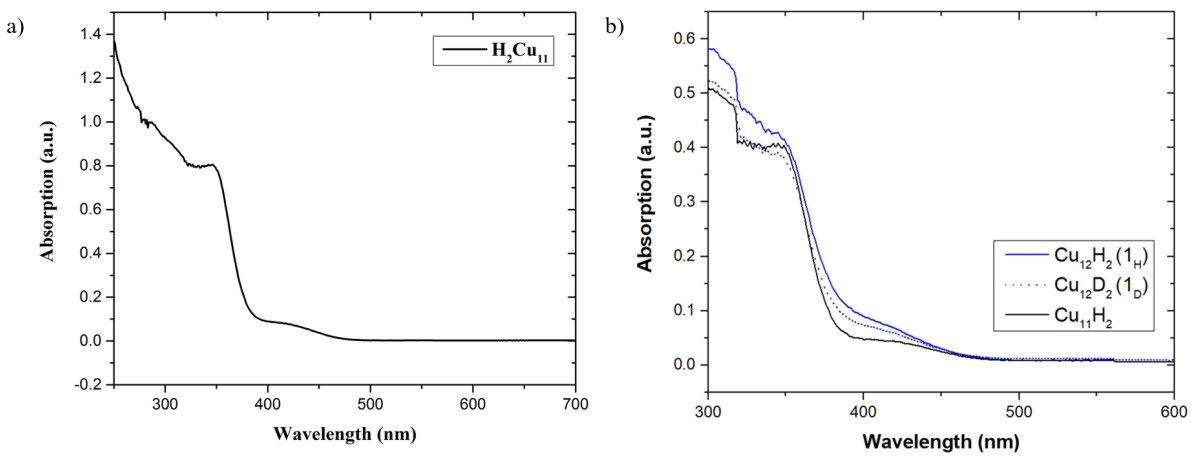

Figure S23. The absorption spectra of cluster a) **H_2Cu_{11}** and b) **1_H**, **1_D**, and **H_2Cu_{11}** in dichloromethane ($1.07x10^{-5}$ M) at ambient temperature.

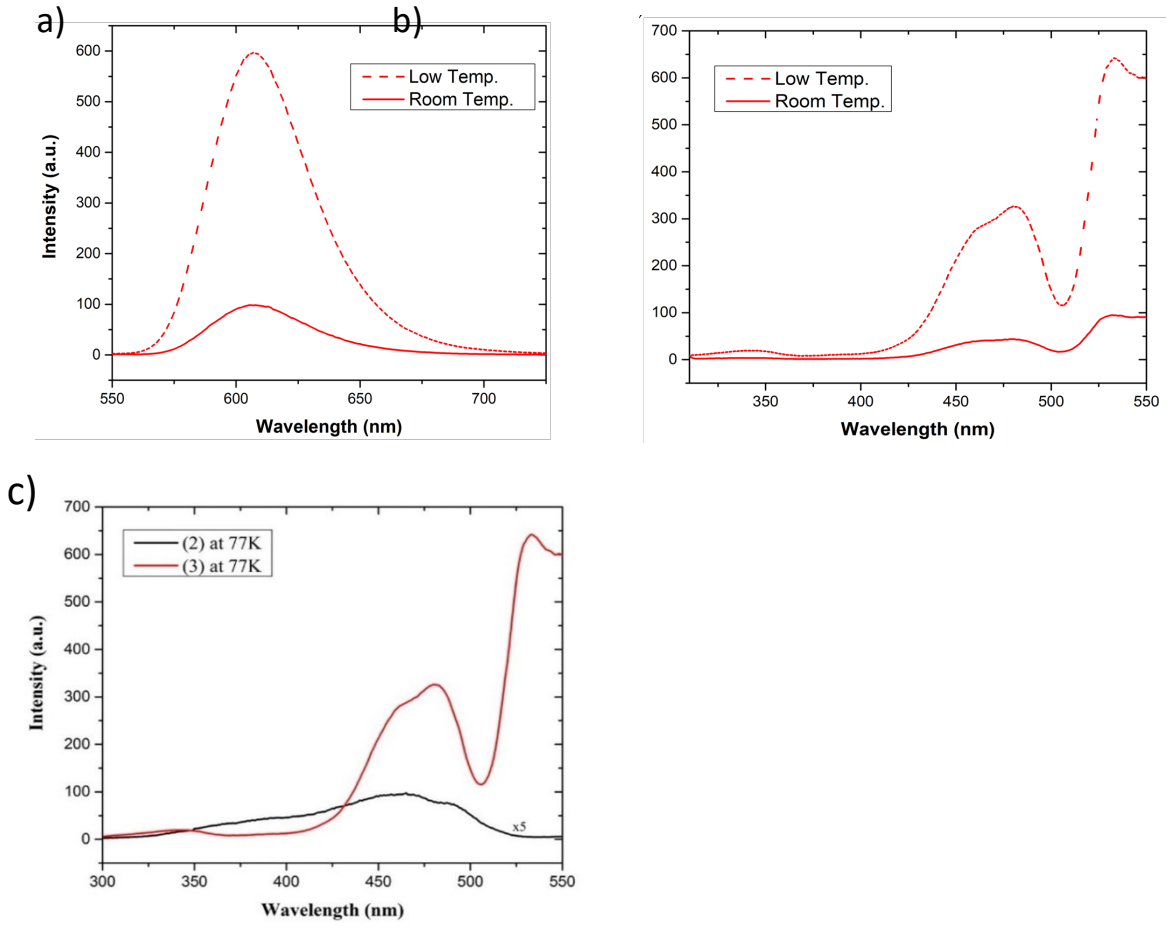

Figure S24. The a) emission and b) excitation spectra of cluster **3** in 2-MeTHF at 77K and ambient temperature. c) excitation spectra of clusters **2** and **3** in 2-MeTHF at 77K.

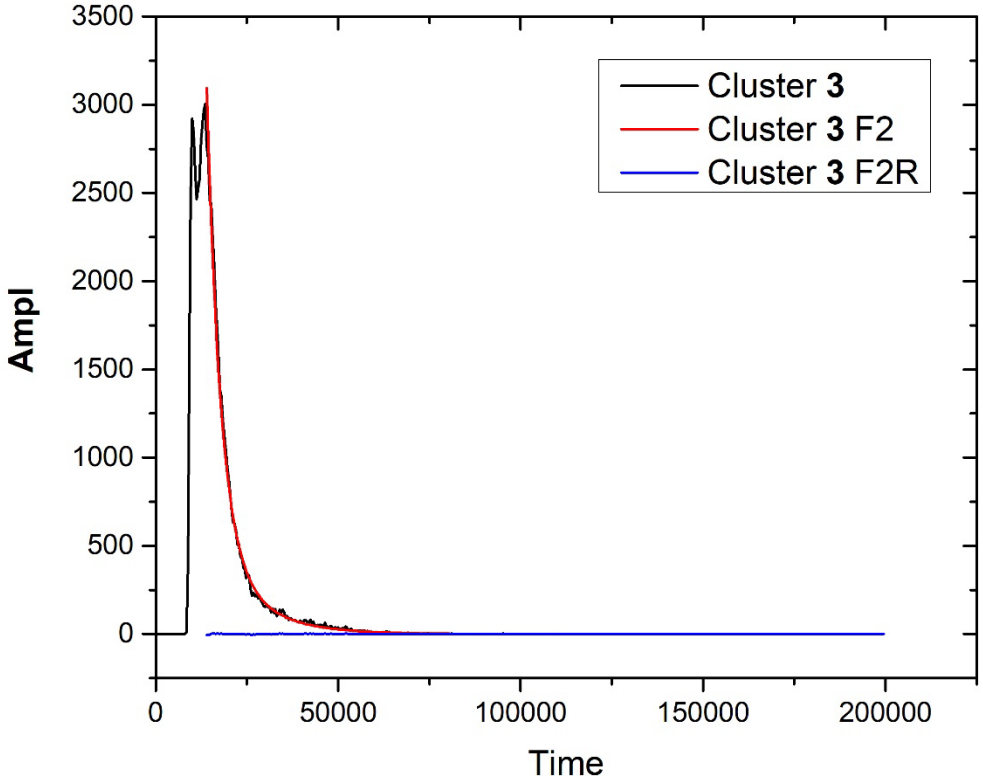

Figure S25. The emission lifetime of cluster **3** at ambient temperature.

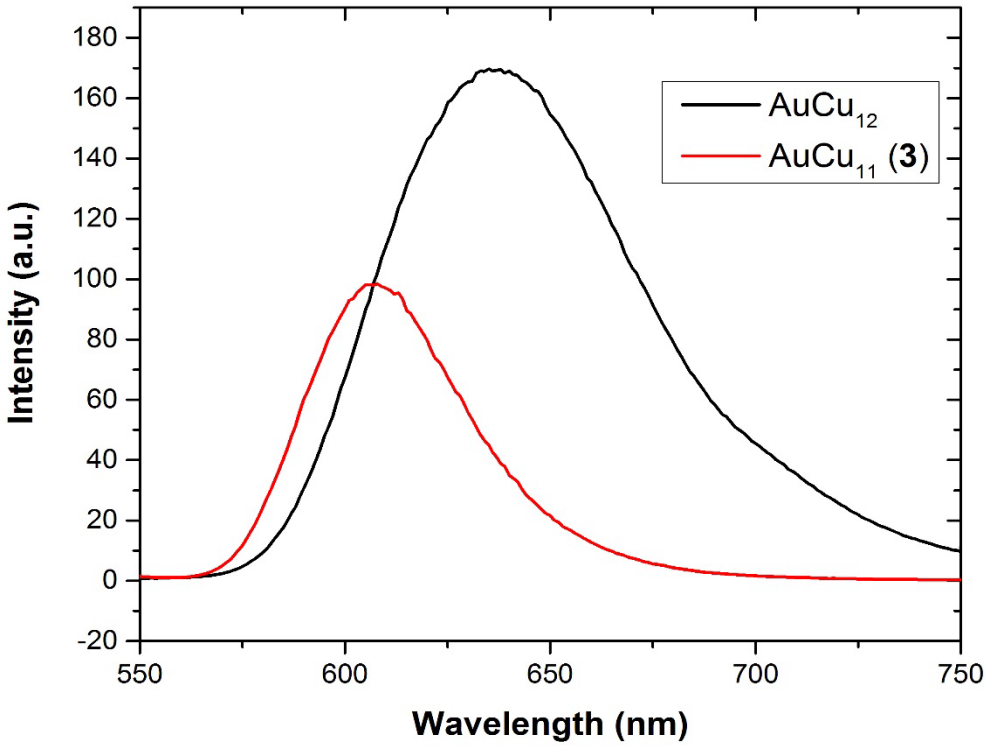

Figure S26. The emission spectra of cluster **3** and **AuCu$_{12}$** in 2-MeTHF at ambient temperature.

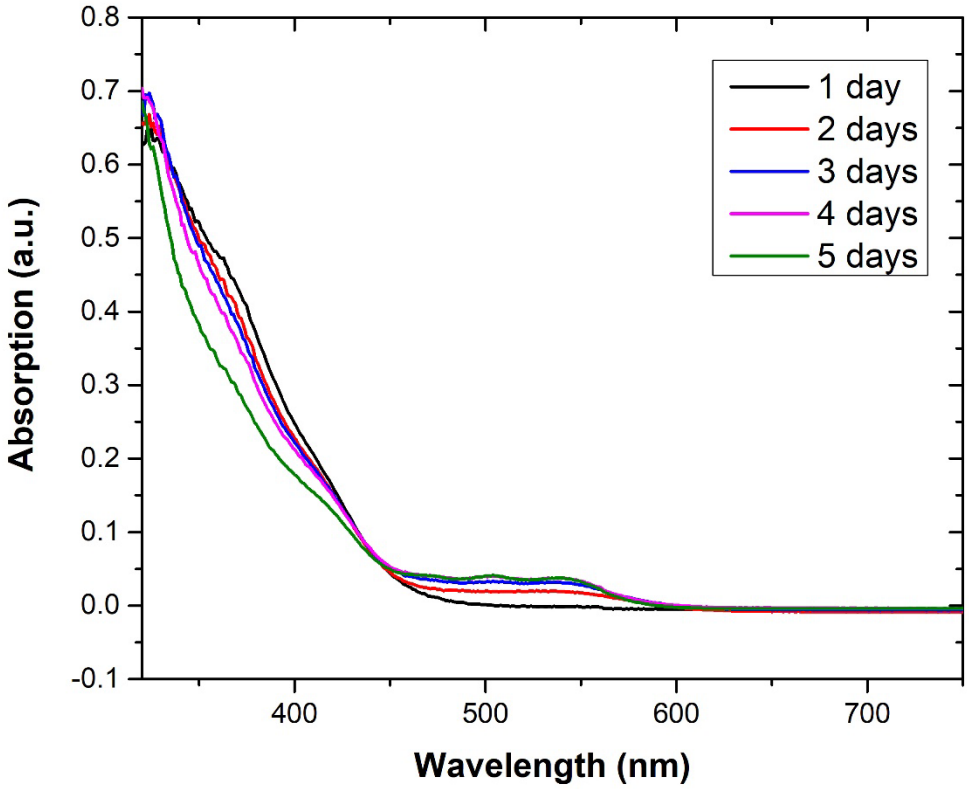

Figure S27. The time-dependent UV-vis absorption spectra of cluster **1** in CH_2Cl_2.

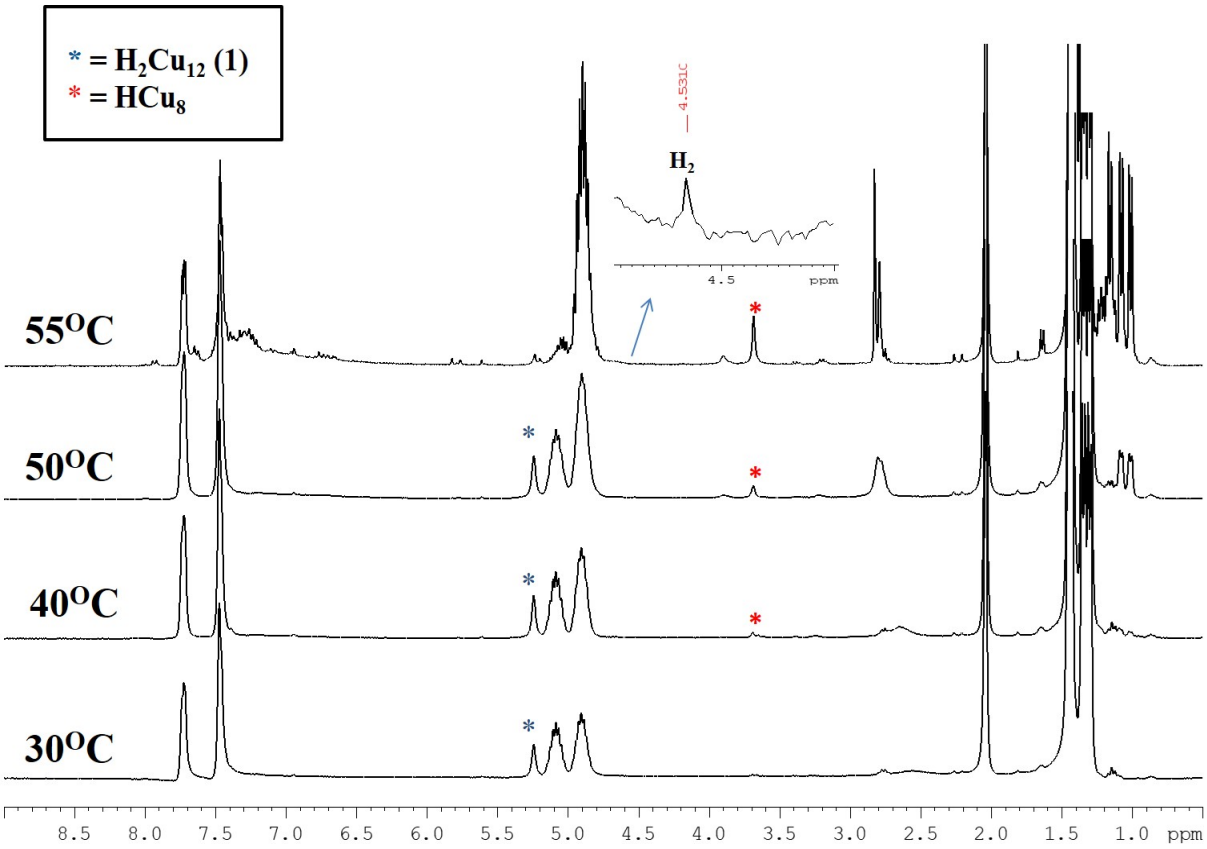

Figure S28. VT ^{1}H NMR spectra of cluster **1** in d_6-acetone.

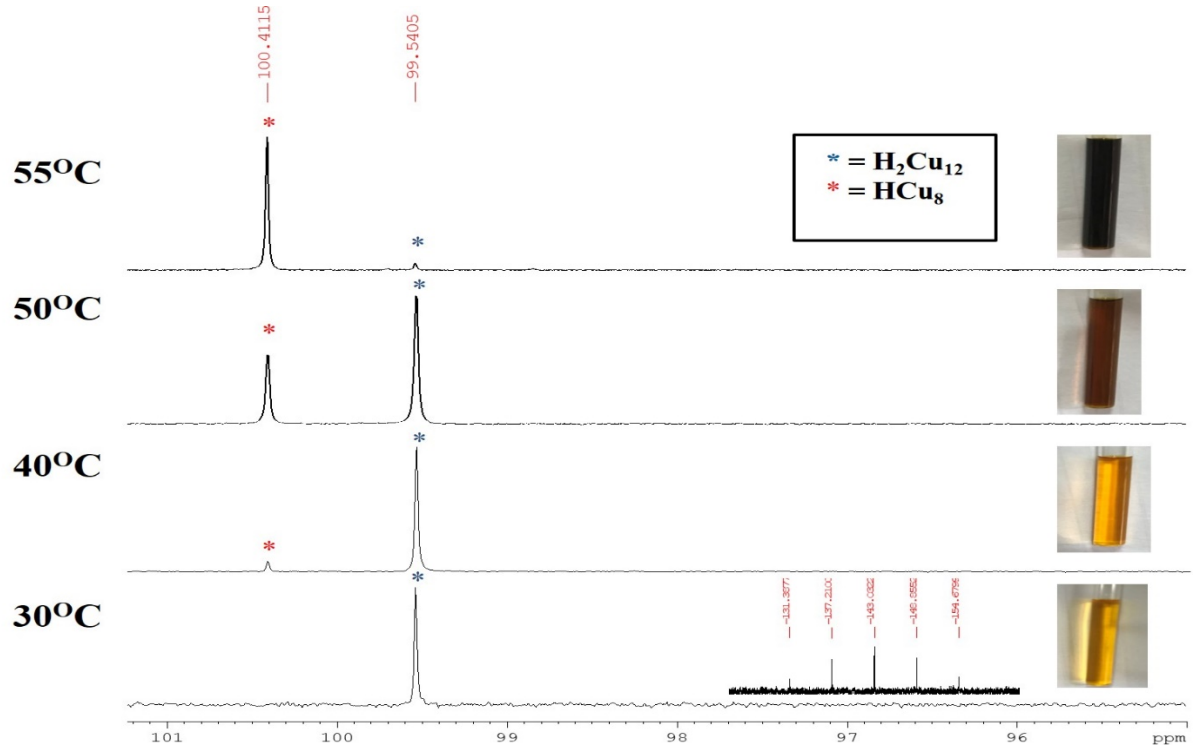

Figure S29. VT $^{31}P\{^{1}H\}$ NMR spectra of cluster **1** in d_6-acetone.

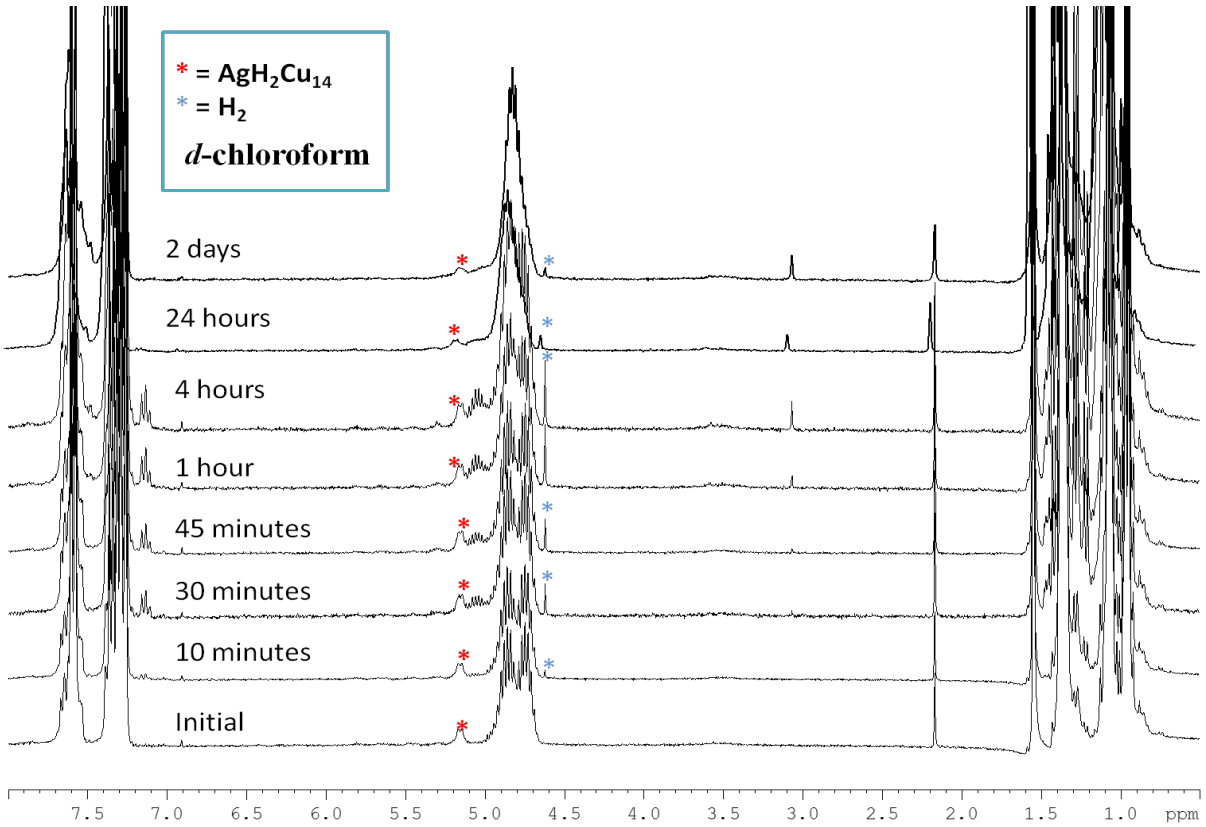

Figure S30. Degradation of cluster **2** into **5** under daylight in $CDCl_3$ monitored by time-dependent ^{1}H NMR spectroscopy.

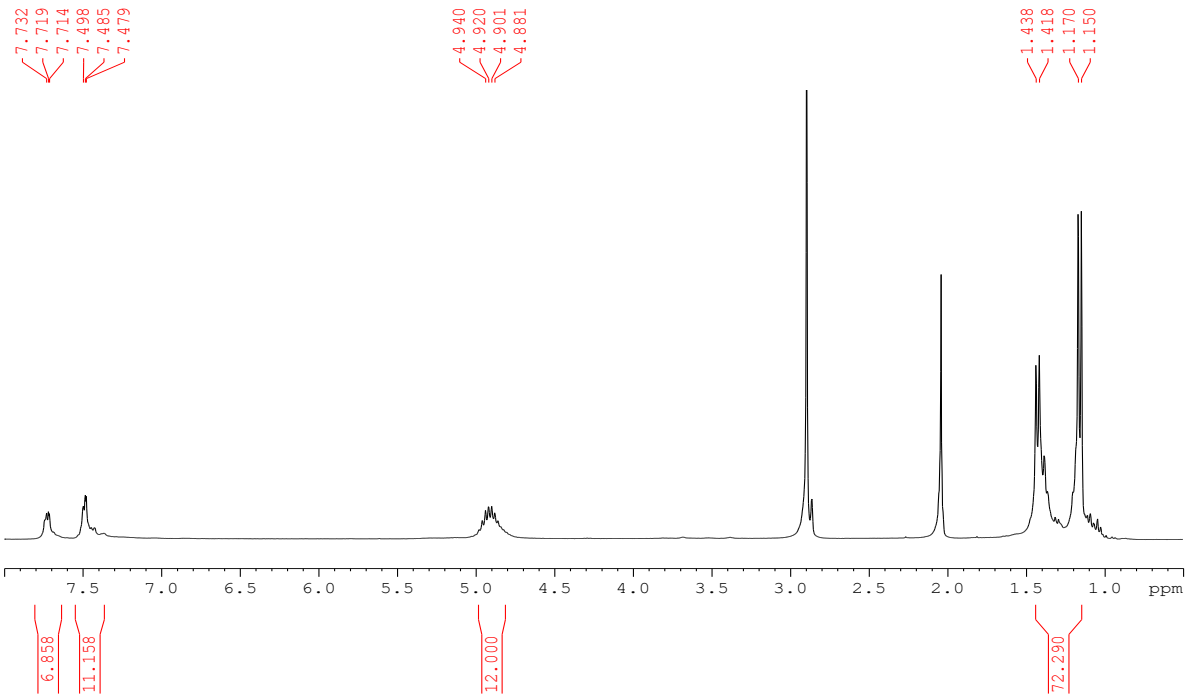

Figure S31. ^{1}H NMR spectrum of cluster **5** in d_6-acetone.

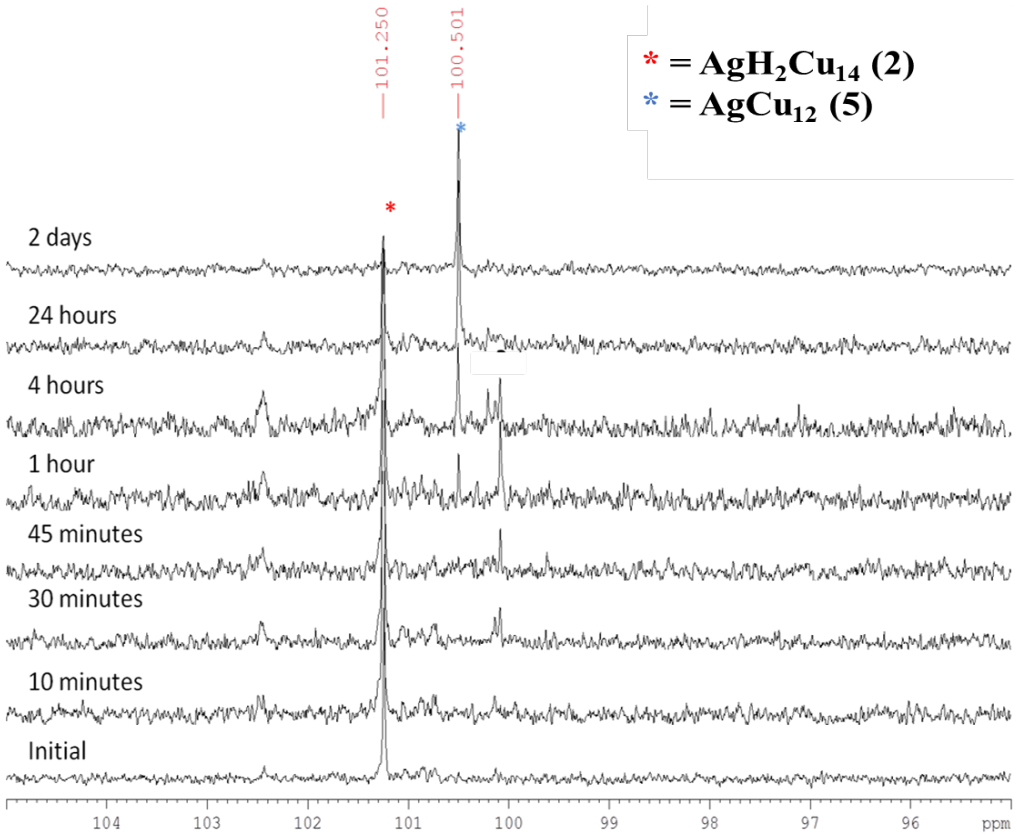

Figure S32. Degradation of cluster **2** into **5** under daylight in $CDCl_3$ monitored by time-dependent $^{31}P\{^{1}H\}$ NMR spectroscopy.

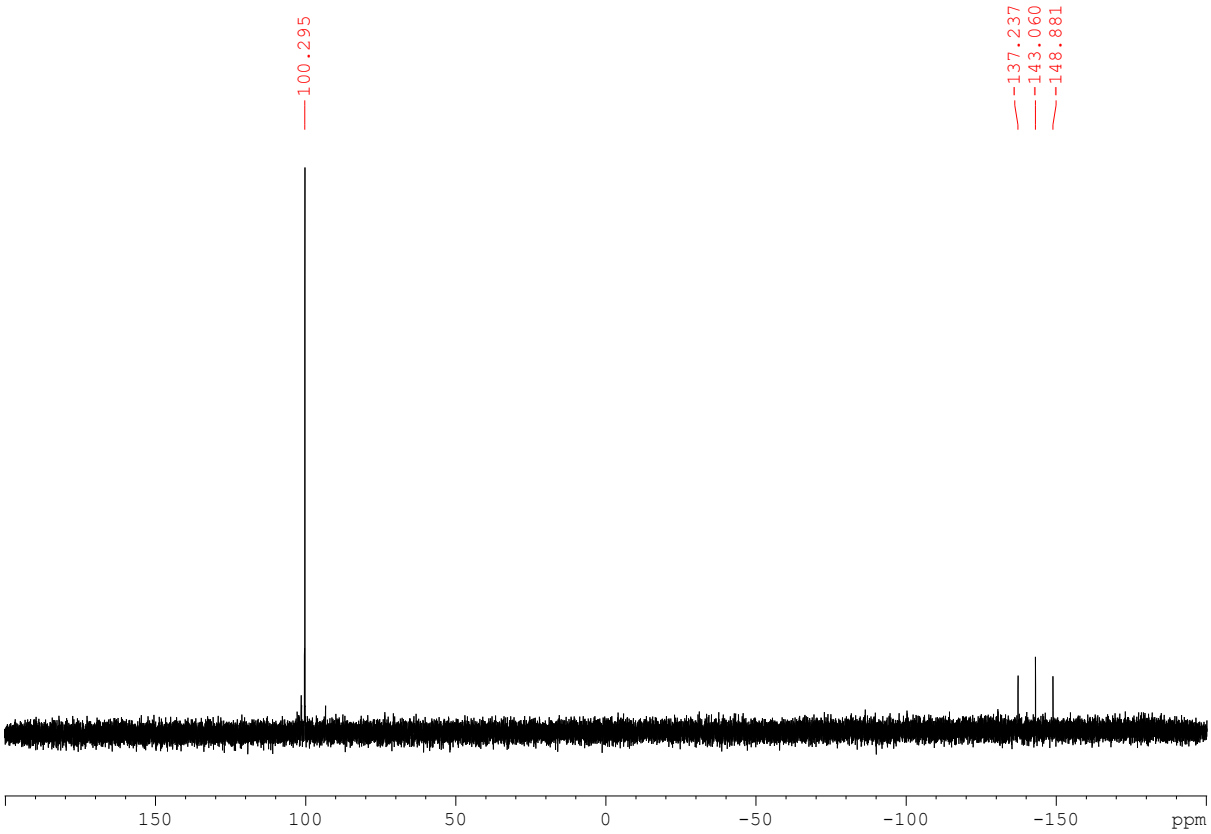

Figure S33. $^{31}P\{^{1}H\}$ NMR spectrum of cluster **5** in d_6-acetone.

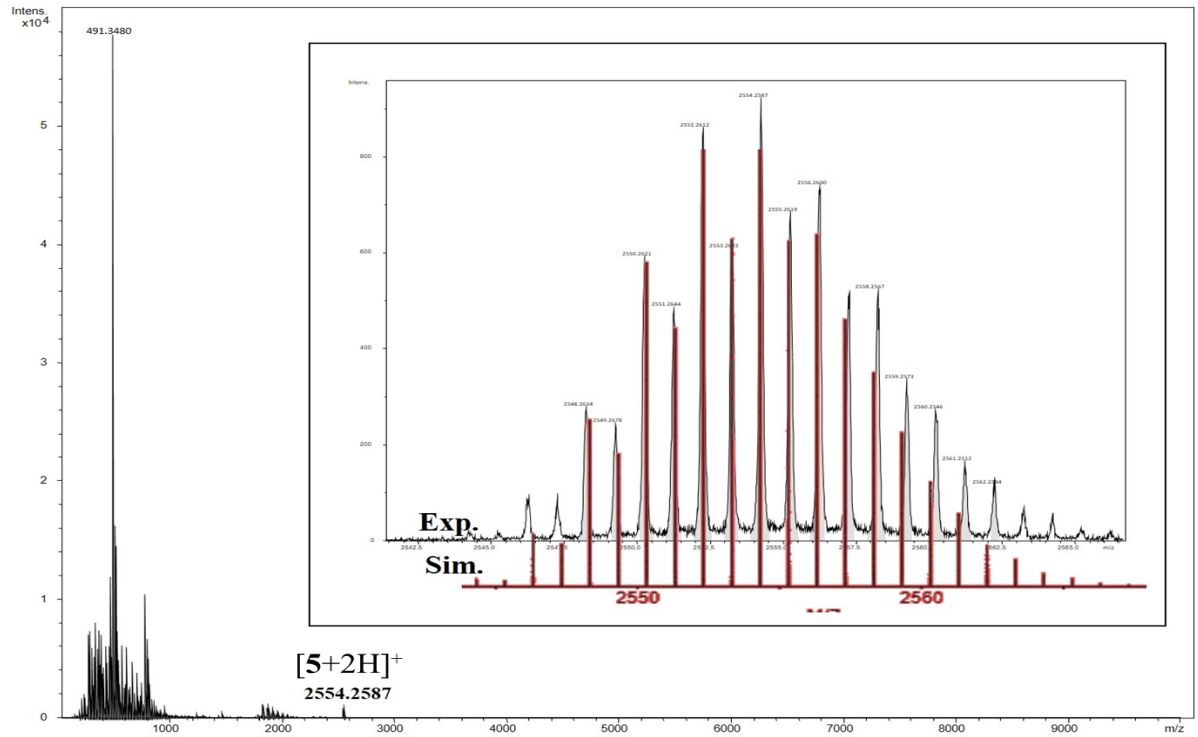

Figure S34. Positive-mode ESI-MS of degradation product $[\mathbf{5}+2H]^+$; inset show experimental (black) and simulated (red) isotopic distribution pattern.

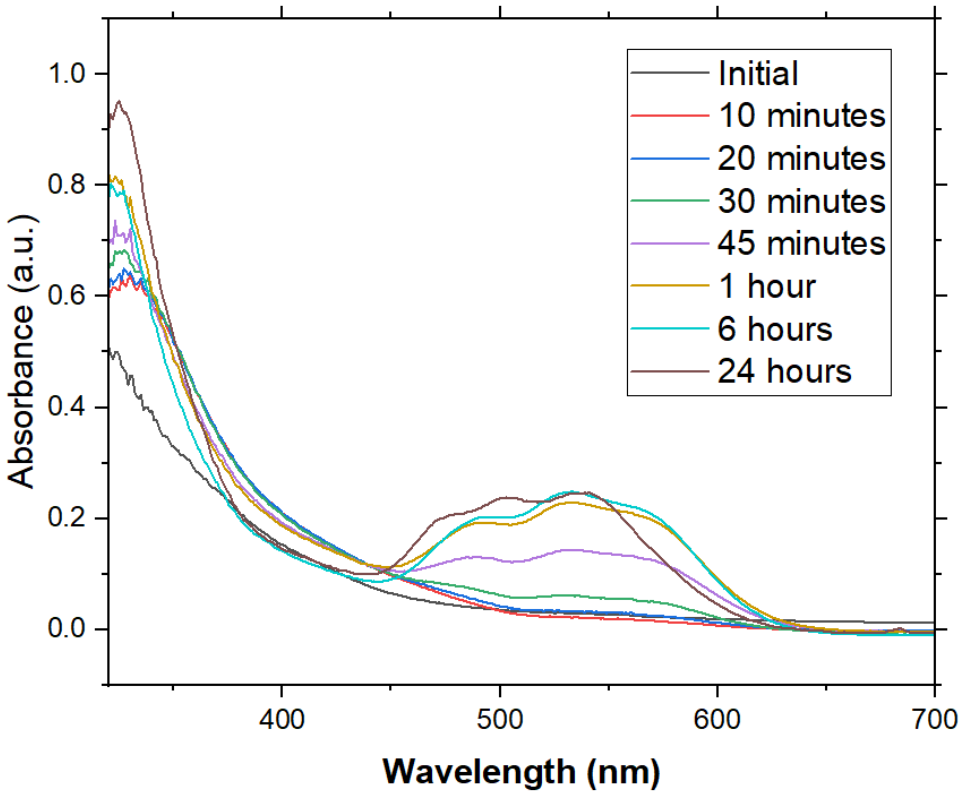

Figure S35. The time-dependent UV-vis absorption spectra cluster **2** in CH_2Cl_2 under light.

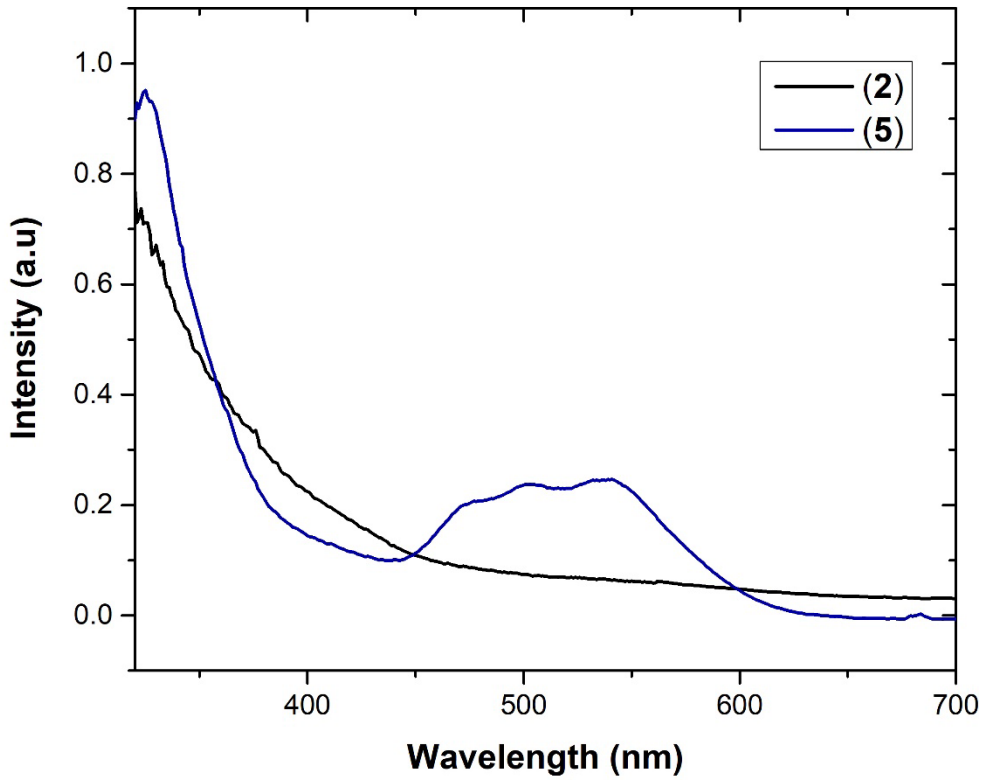

Figure S36. The comparison UV-vis absorption spectra cluster **2** and **5** in CH_2Cl_2.

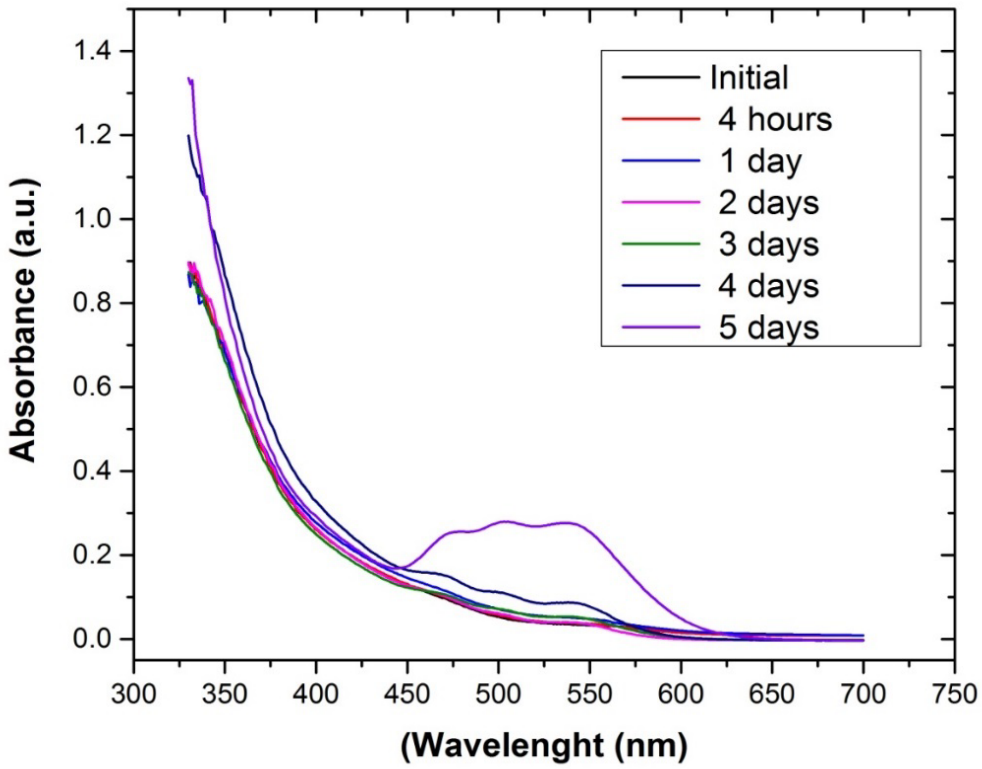

Figure S37. UV-vis absorption spectra of cluster **2** in CH_2Cl_2 in dark condition.

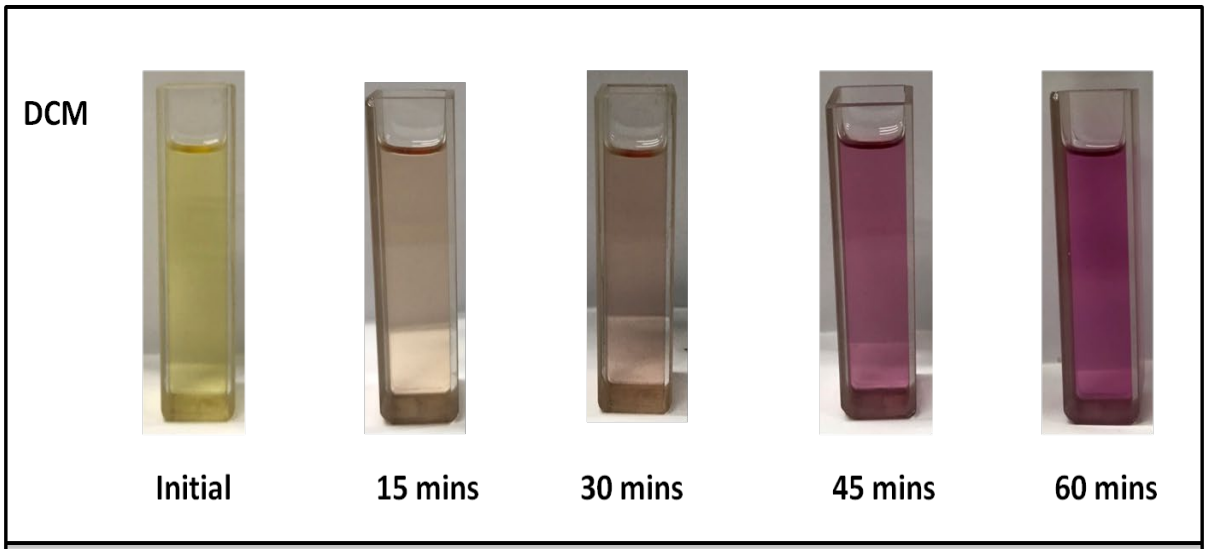

Figure S38. Colour changes from clusters **2** to **5** under daylight in dichloromethane.

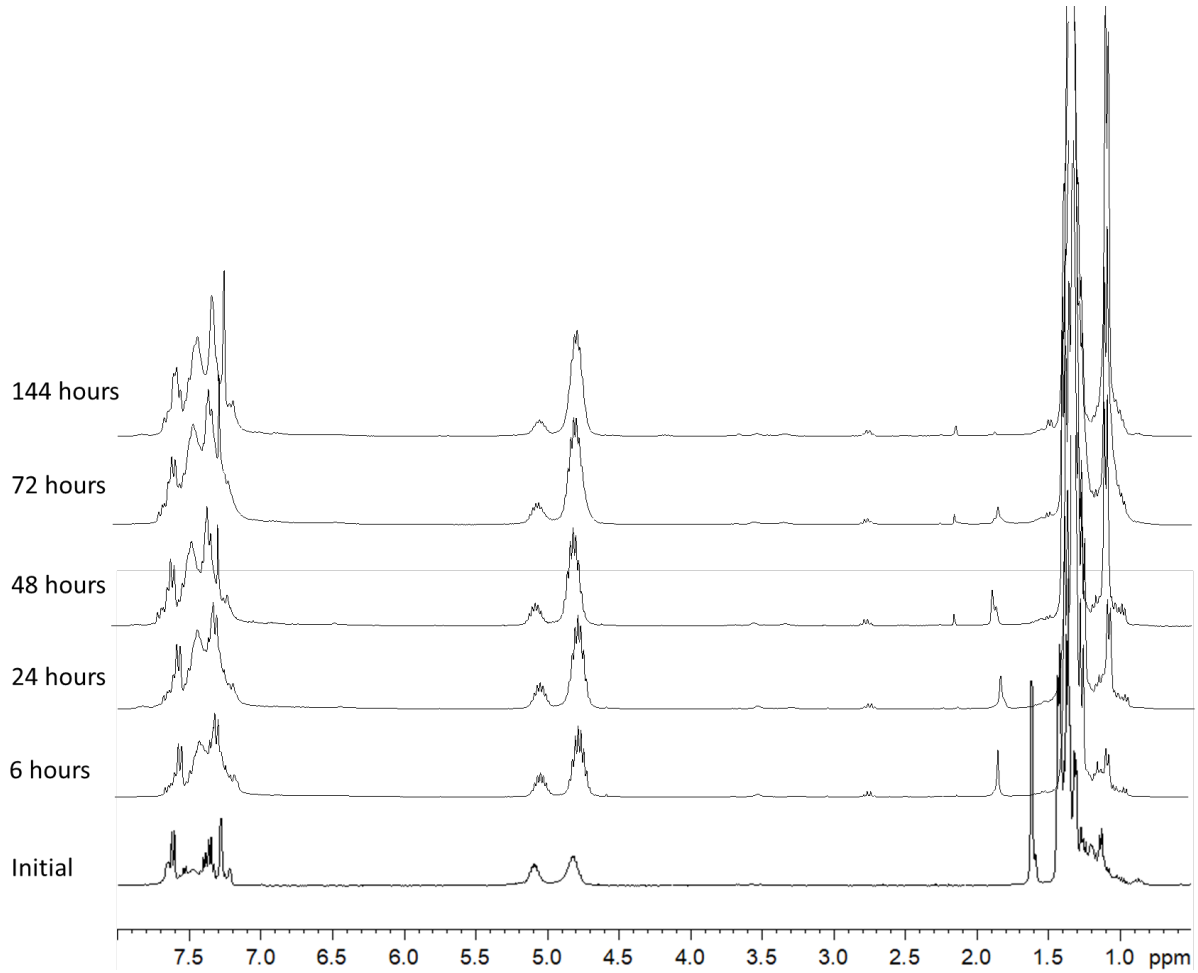

Figure S39. Partial decompositions of cluster **3** into **4** in $CDCl_3$ at ambient temperature monitored by time-dependent of ^1H NMR spectroscopy.

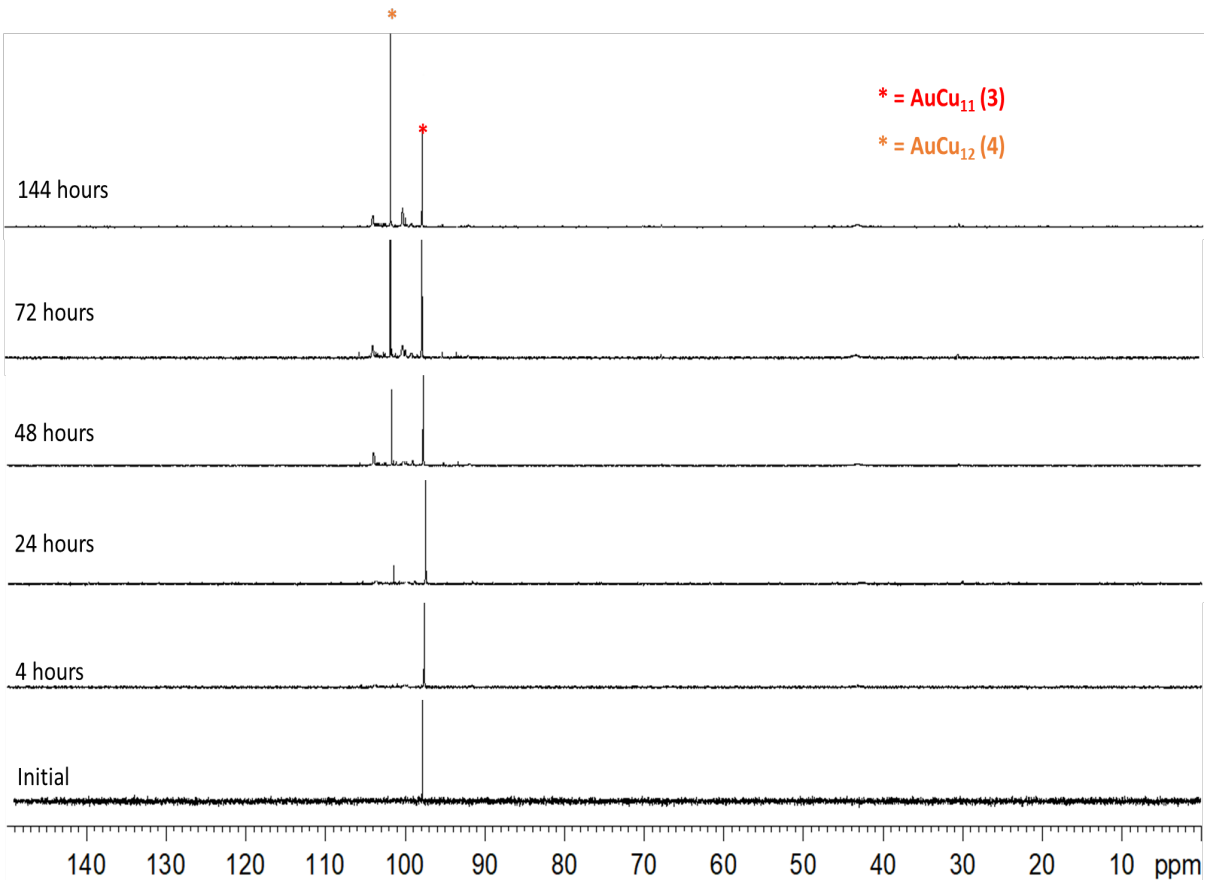

Figure S40. Partial decompositions of cluster **3** into **4** in $CDCl_3$ at ambient temperature monitored by $^{31}P\{^1H\}$ NMR spectroscopy.

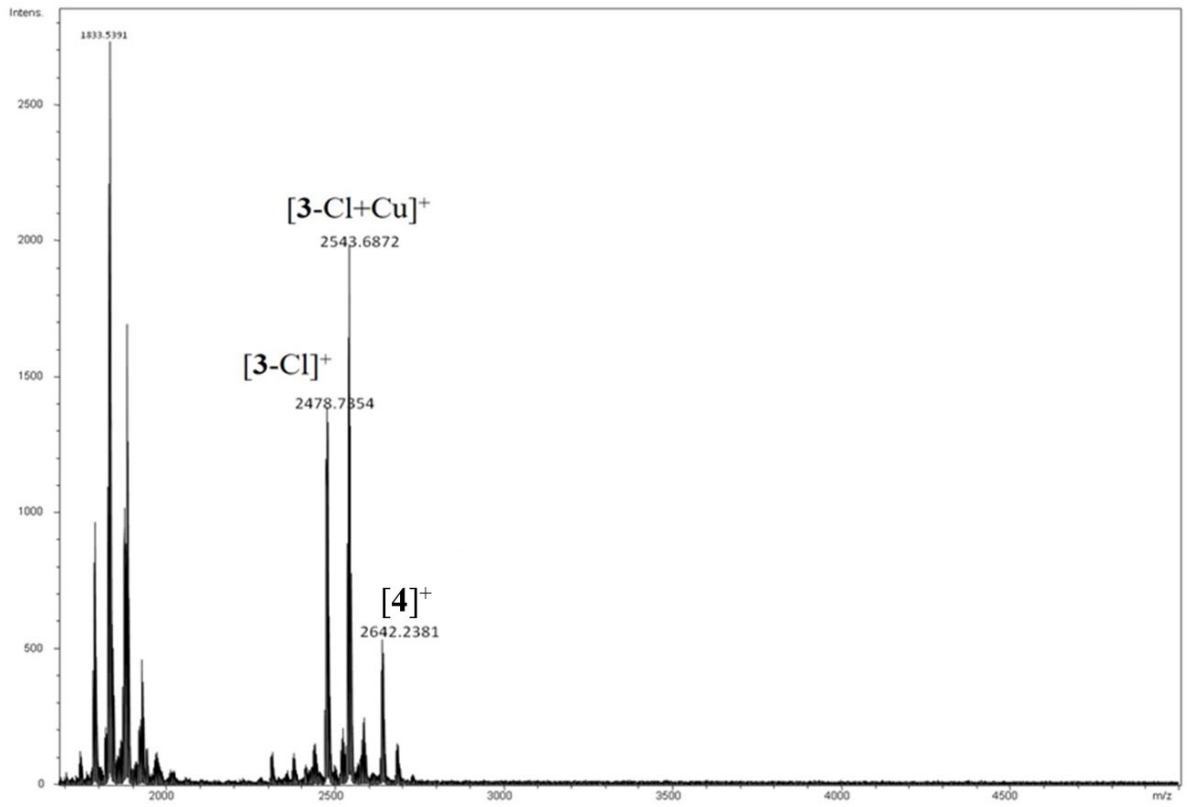

Figure S41. Positive-mode ESI-MS depicts the decomposition of cluster **3** to two-electron superatom $[\mathbf{4}]^+$.

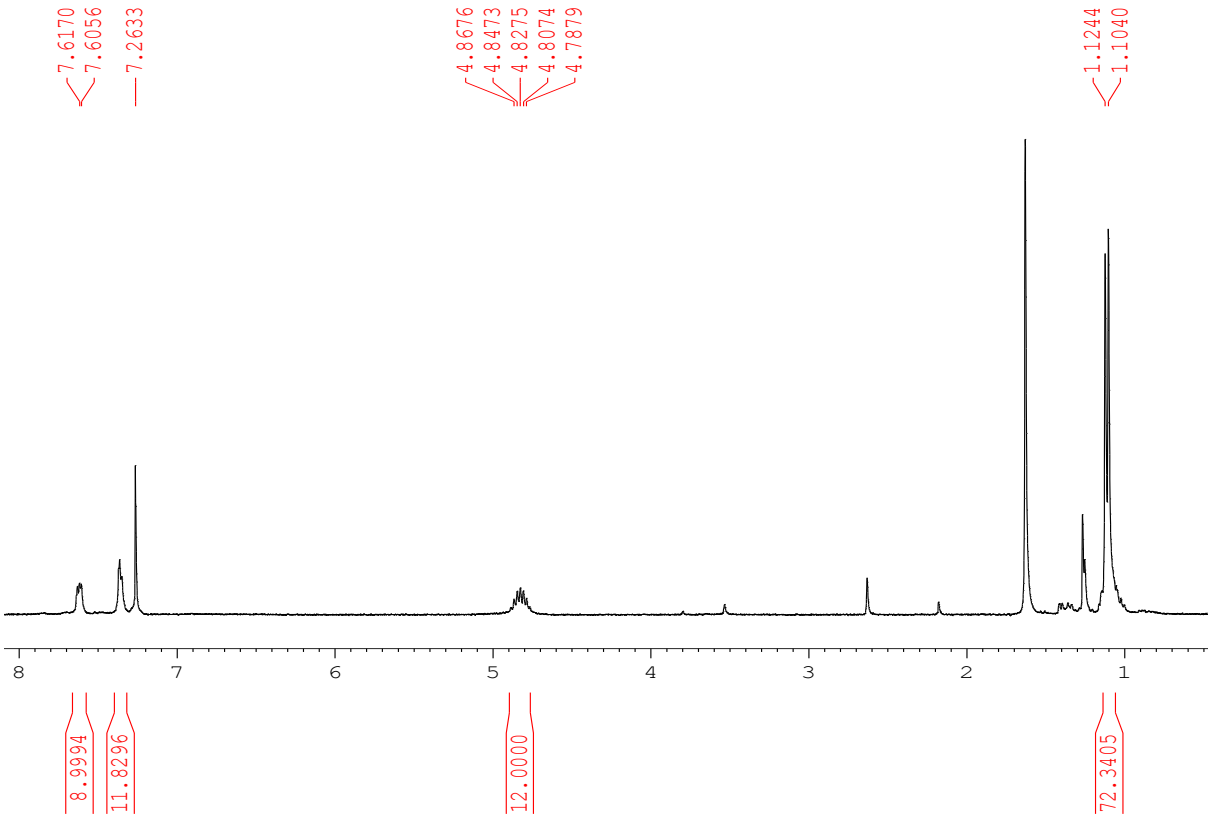

Figure S42. ^{1}H NMR spectrum of cluster $[\mathbf{4}]^+$ in $CDCl_3$.

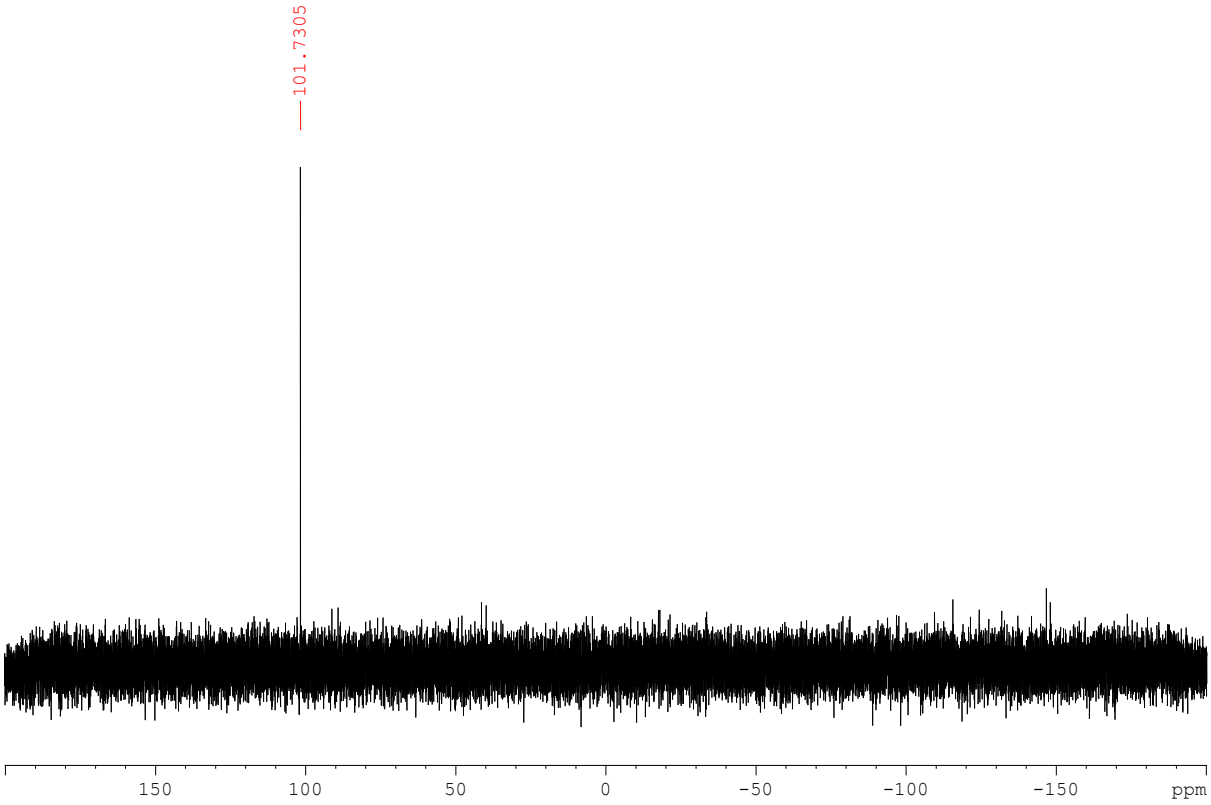

Figure S43. $^{31}P\{^{1}H\}$ NMR spectrum of cluster $[\mathbf{4}]^{+}$ in $CDCl_3$.

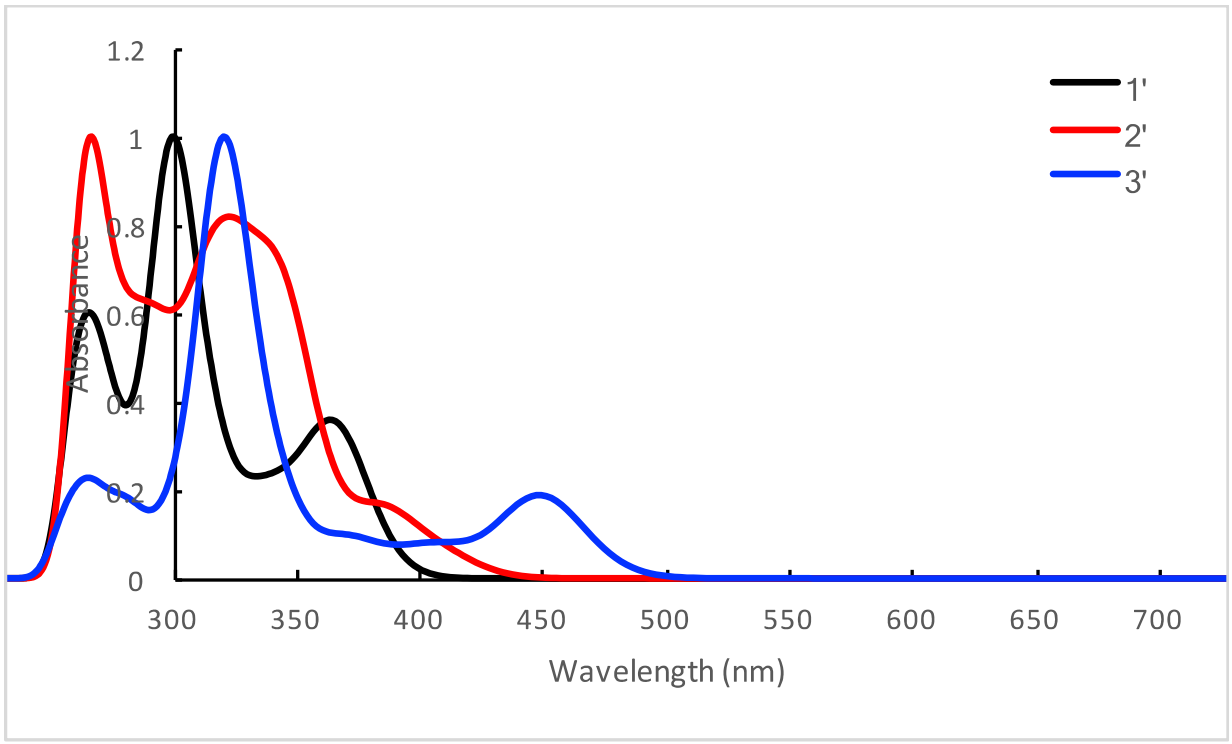

Figure S44. The TDDFT-simulated spectra of **1'**, **2'**, and **3'**. (normalized absorbances)

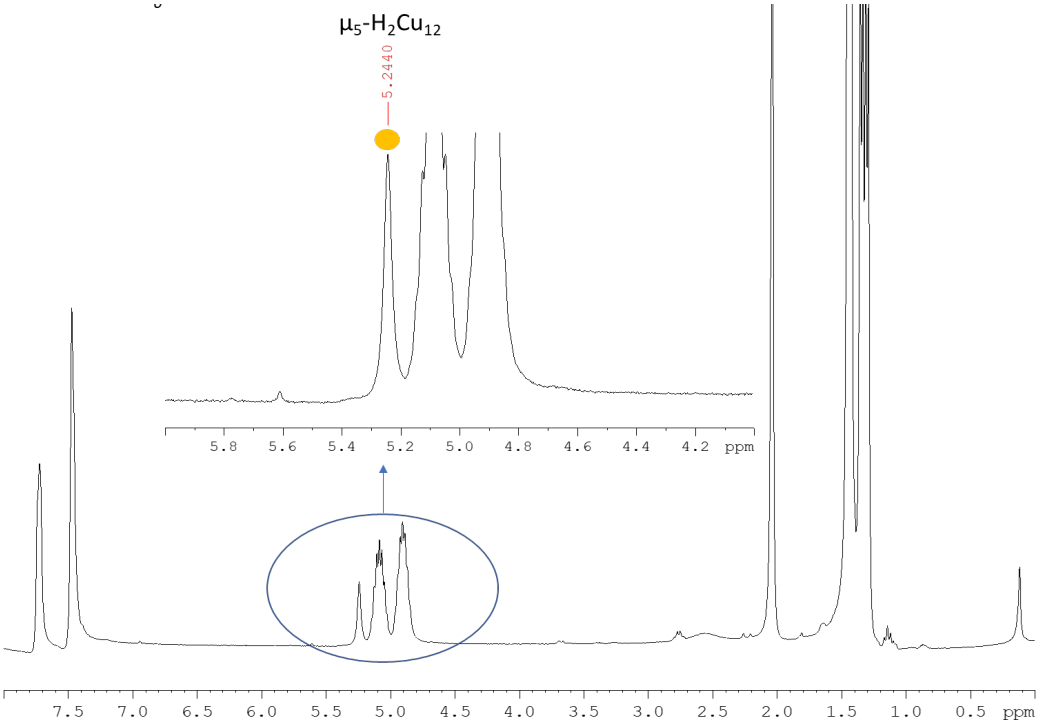

Figure S45. The ^{1}H NMR spectra of 1:1 mixture of $Cu_{11}H_2$ and $Cu_{11}D_2$ with Cu^{+} ions in *d*$_6$-acetone. (Inset: the expanding ^{1}H NMR spectra of **1** from 4.0-6.0 ppm)

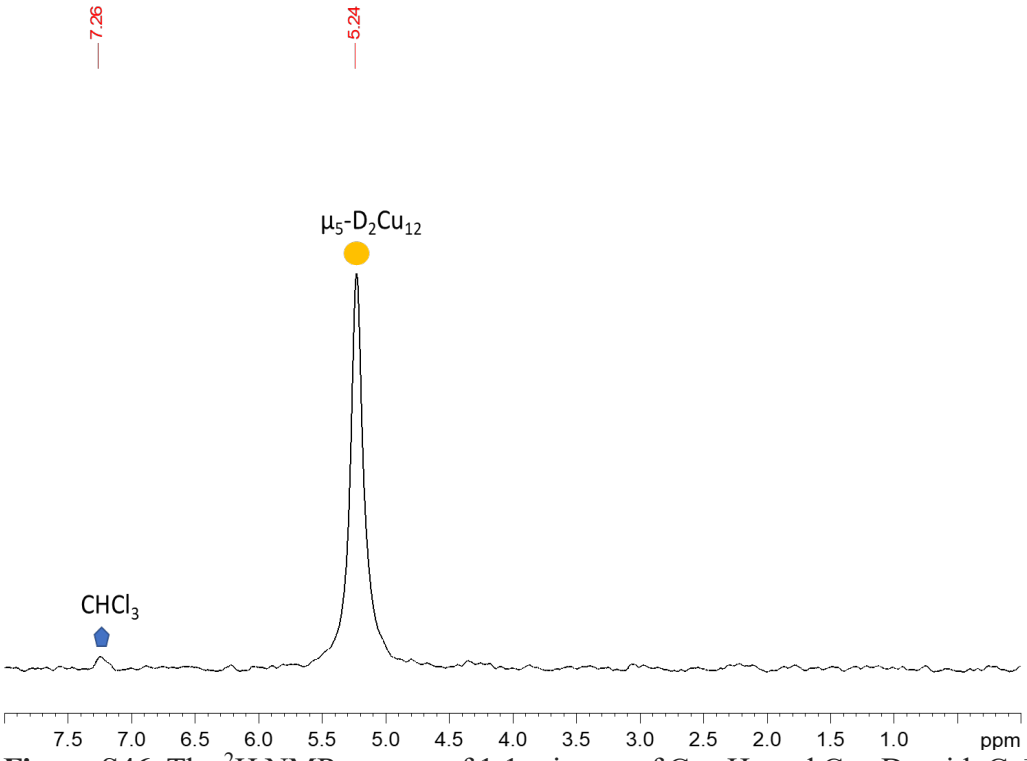

Figure S46. The ^{2}H NMR spectra of 1:1 mixture of $Cu_{11}H_2$ and $Cu_{11}D_2$ with Cu^{+} ions.

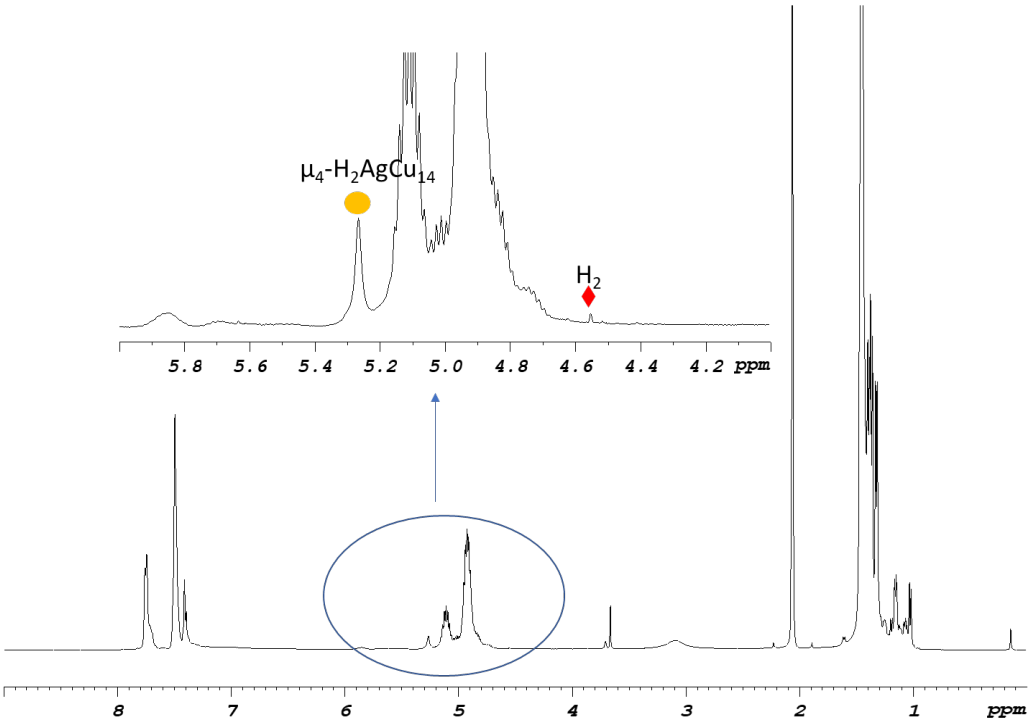

Figure S47. The ^{1}H NMR spectra of 1:1 mixture of $Cu_{11}H_2$ and $Cu_{11}D_2$ with Ag^{+} ions in d_6-acetone. (Inset: the expanding ^{1}H NMR spectra of **2** from 4.0-6.0 ppm)

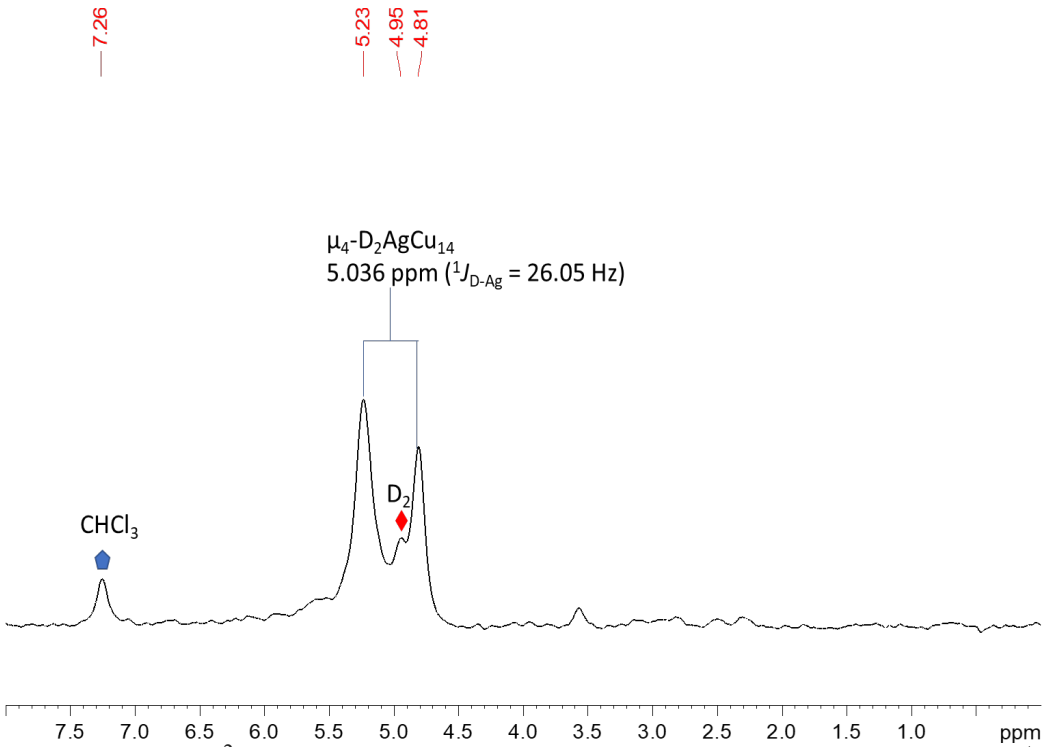

Figure S48. The ^{2}H NMR spectra of 1:1 mixture of $Cu_{11}H_2$ and $Cu_{11}D_2$ with Ag^{+} ions.

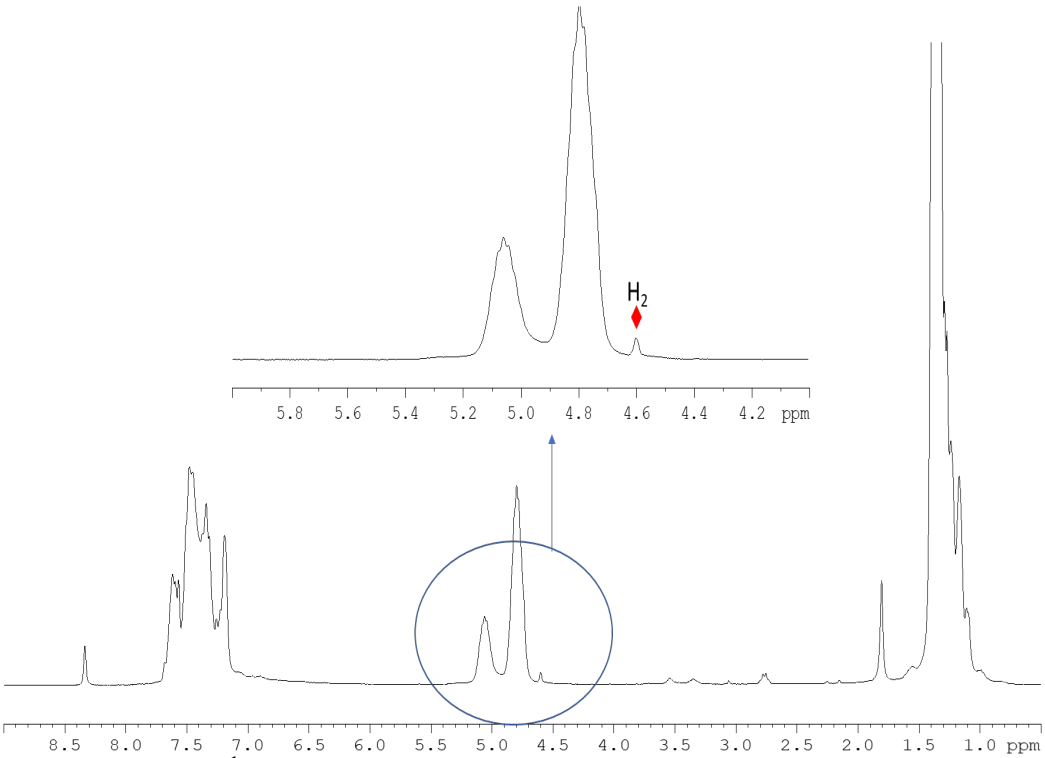

Figure S49. The ^{1}H NMR spectra of 1:1 mixture of $Cu_{11}H_2$ and $Cu_{11}D_2$ with Au^{+} ions in $CDCl_3$. (Inset: the expanding ^{1}H NMR spectra of **3** from 4.0-6.0 ppm)

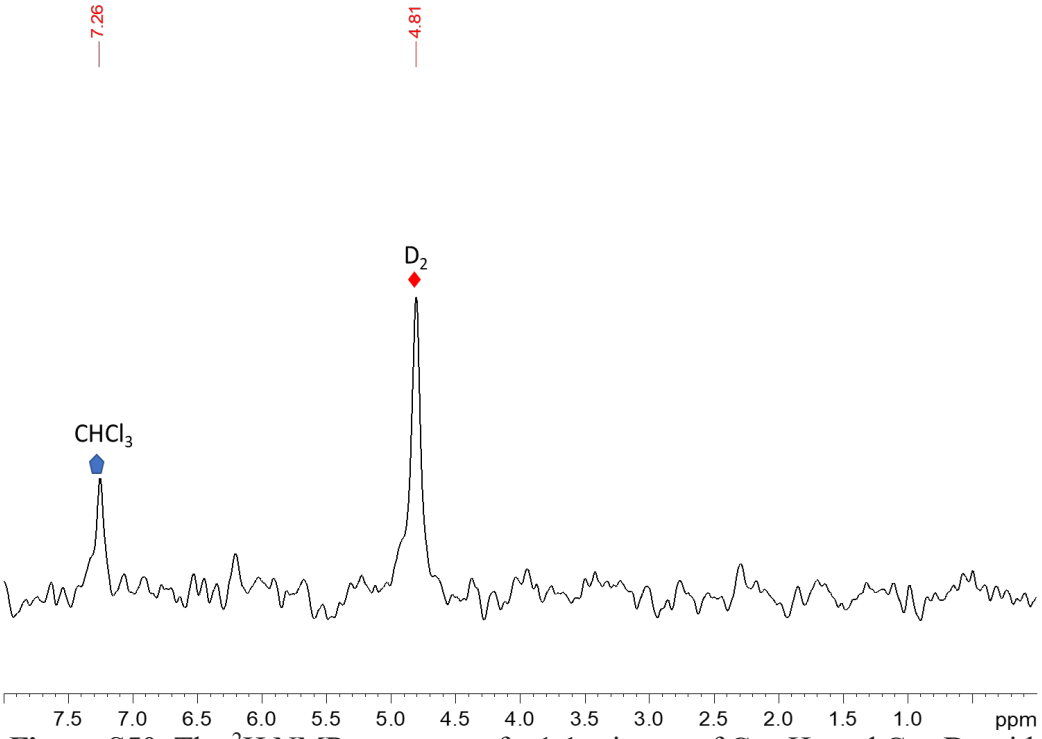

Figure S50. The ^{2}H NMR spectrum of a 1:1 mixture of $Cu_{11}H_2$ and $Cu_{11}D_2$ with Au^{+} ions.

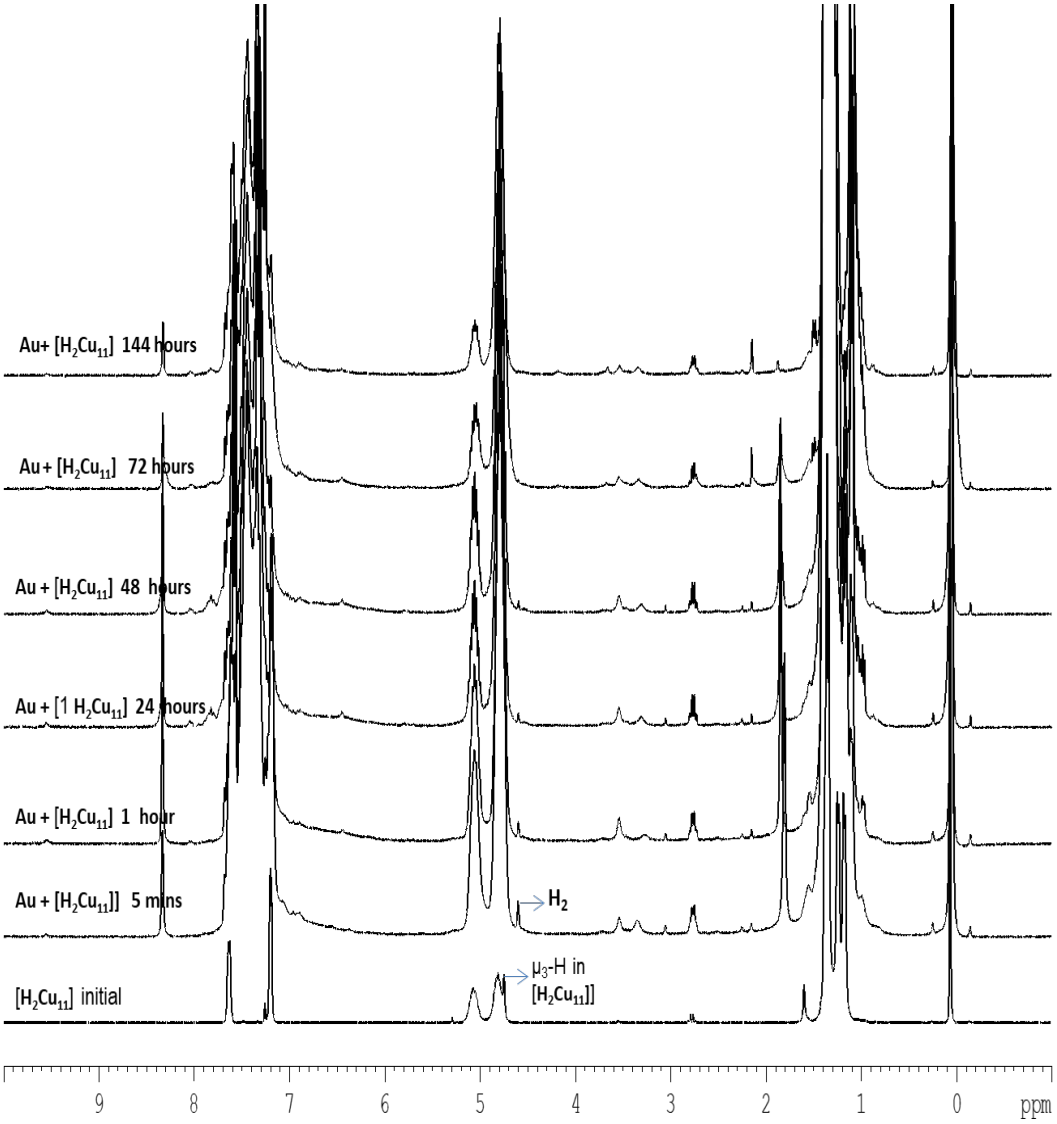

Figure S51. Partial decompositions of cluster **3** into **4** in $CDCl_3$ at ambient temperature monitored by time-dependent ^1H NMR spectroscopy.

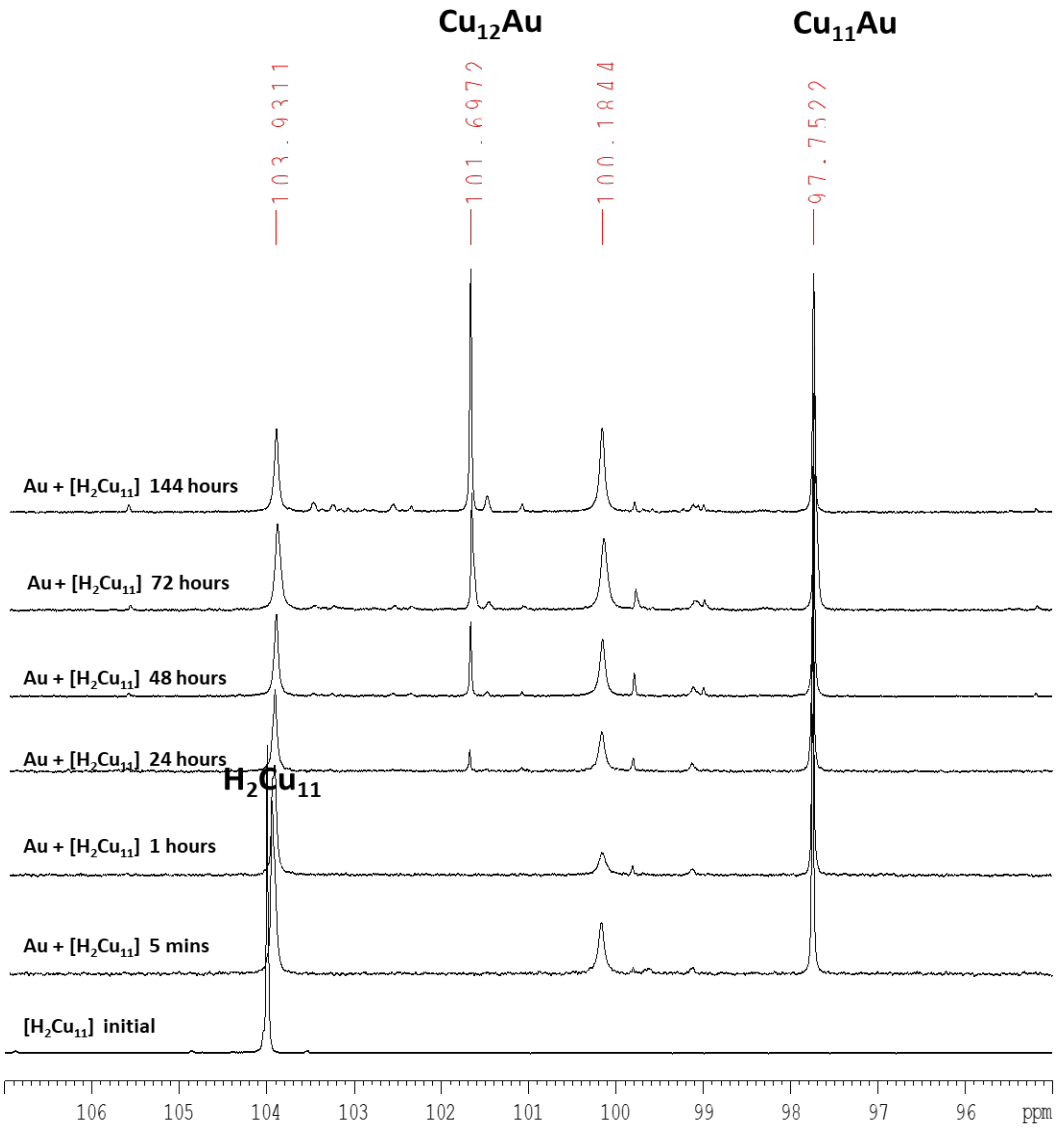

Figure S52. Partial decompositions of cluster **3** into **4** in $CDCl_3$ at ambient temperature monitored by $^{31}P\{^1H\}$ NMR spectroscopy.

Table S1. The chemical shift and coupling constants of **2H** derived from ^{1}H and ^{109}Ag spectra.

^{1}H chemical shift (ppm)	**^{1}H-^{107}Ag (Hz)**	**^{1}H-^{109}Ag (Hz)**	**^{109}Ag chemical shift (ppm)**	**^{1}H-^{109}Ag (Hz)**
5.1519	93.6	107.7	1279.5	107.7

Table S2. The chemical shift and coupling constants of **2D**.

^{2}H chemical shift (ppm)	**^{2}H-^{107}Ag (Hz)**	**^{2}H-^{109}Ag (Hz)**
5.151	14.4	16.5

Table S3. Selected X-ray crystallographic data of **1**, **2**, and **3**.

	1.PF$_6$	**2.PF$_6$**	**3**
CCDC no.	2095375	2095376	2095378
Empirical formula	$C_{60}H_{101}Cu_{12}F_6O_{12}P_7S_{12}$	$C_{177}H_{250}Ag_2Cu_{28}F_{12}O_{27}P_{14}S_{24}$	$C_{60}H_{99}AuClCu_{11}O_{12}P_6S_{12}$
Formula weight	2492.39	6235.64	2514.28
Temperature, K	150(2)	100(2)	150(2)
Wavelength, Å	0.71073	0.71073	0.7103
Crystal system	Orthorhombic	Triclinic	Triclinic
Space group	*P*bca	*P*(-)1	*P*(-)1
a, Å	25.4321(10)	14.4641(17)	14.4079(12)
b, Å	26.7372(10)	15.546(3)	17.0567(15)
c, Å	27.2015(10)	28.242(4)	19.5459(16)
α, deg.	90	100.713(4)	92.092(2)
β, deg.	90	95.769(3)	107.322(2)
γ, deg.	90	107.040(2)	92.615(2)
Volume, Å^3	18496.6(12)	5884.1(15)	4574.57(7)
Z	8	1	2
ρ, Mg m^{-3}	1.790	1.790	1.825
μ, mm^{-1}	3.152	3.004	4.553
Crystal size, mm^3	0.15 x 0.13 x 0.05	0.40 x 0.16 x 0.06	0.09 x 0.09 x 0.08
θ_{max}, deg.	26.415	25.000	25.000
Reflections collected / unique	153228 / 18980 (R_{int} = 0.0487)	33926 / 20388 (R_{int} = 0.0215)	26677 / 15895 (R_{int} = 0.0296)
Completeness, %	100	98.3	98.7
restraints / parameters	0 / 1014	700 / 1354	3 / 972
GOF	1.128	1.028	1.021
[a]*R*1, [b]*wR*2 [I>2σ(I)]	*R*1 = 0.0344, *wR*2 = 0.0735	*R*1 = 0.0411, *wR*2 = 0.1091	*R*1 = 0.0477, *wR*2 = 0.1276
[a]*R*1, [b]*wR*2 (all data)	*R*1 = 0.0546, *wR*2 = 0.0842	*R*1 = 0.0501, *wR*2 = 0.1186	*R*1 = 0.0680, *wR*2 = 0.1465
Largest diff. peak / hole, e Å^{-3}	1.557, -0.918	1.689, -1.285	2.111, -2.156

[a] $R1 = \Sigma \mid\mid F_o \mid - \mid Fc \mid\mid / \Sigma \mid F_o \mid$. [b] $wR2 = \{\Sigma[w(F_o^2 - F_c^2)^2]/\Sigma[w(F_o^2)^2]\}^{1/2}$.

Table S4. 298 K absorption, emission, and lifetime of **3** ($AuCu_{11}$) and **4** (**$AuCu_{12}$**)

Compound	λ_{max}(nm) [$\varepsilon(M^{-2a}m^{-1})$]	λ_{em} (nm)	Lifetime, $\tau(\mu s)$ One-exp[a]	Φ_{em}[b]	k_{obs}, $1/\tau(\mu s^{-1})$; one-exp	k_{RAD}[c] (μs^{-1})	k_{NRD}[d] (μs^{-1})
$AuCu_{11}$ (3)	325, 384, 435, 495, 550 [7840]	606	3.75	0.033	0.27	0.009	0.26
$AuCu_{12}$ (4)	326, 433 480,540 [8510]	637	3.20	0.32	0.31	0.10	0.21

[a] mean emission lifetime (τ). [b]emission quantum yield (see page S1(SI)). [c]$\Phi_{em} = k_{RAD}/k_{obs}$, k_{RAD} = radiative rate constant and k_{obs} = mean excited-state decay rate constant. [d]$k_{obs} = k_{RAD} + k_{NRD}$, k_{NRD} = nonradiative rate constant.

Table S5. Selected DFT-computed data for the considered hydride clusters

		$Cu_{11}H_2$'	**1'**	**2(Cu)'**	**2'**
HOMO-LUMO gap (eV)		3.72	4.19	3.87	3.87
Interatomic distances (Å) and Wiberg indices (avg. values)	M_{cent}-H	-	1.638 [0.217]	1.746 [0.153]	2.064 [0.129]
	$Cu_{top/cap}$-H	1.888 [0.070]	1.888 [0.036]	2.448 [0.011]	2.028 [0.036]
	Cu_{tri}-H	1.749 [0.097]	1.994 [0.049]	-	-
	Cu_{ico}-H	-	-	1.821 [0.077]	1.855 [0.079]
NAO charges (avg. values)	$Cu_{top/cap}$	0.74	0.72	0.66	0.66
	Cu_{tri}	0.68	0.76	-	-
	Cu_{ico}	-	-	0.77	0.80
	H (hydride)	-0.69	-0.66	-0.64	-0.63
	$M_{cent}H_2$ unit	-	-0.88	-1.02	-1.22

Table S6. Neutron crystallographic data of $\mathbf{2_N}$.

CCDC no.	2095377
formula	$C_{84}H_{116}AgCu_{14}F_6O_{12}P_7S_{12}$
formula weight	3030.70
crystal system	Monoclinic
space group	$P2_1/c$
a (Å)	25.8195(16)
b (Å)	16.0651(14)
c (Å)	27.1311(15)
α (deg)	90
β (deg)	102.683(5)
γ (deg)	90
V (Å^3)	10979.2(13)
Z	4
T (K)	20(2)
Crystal size (mm)	4.20 x 3.75 x 2.90
λ (Å)	0.43 – 3.50
ρ (Mg m^{-3})	1.834
μ (cm^{-1})	0.11237 + 0.08375λ
measured reflns. / unique	35886 / 9151
restraints / no. of params. refined	54 / 1955
R1[a] (observed), *w*R2[b] (all)	0.0543, 0.1301
GOF	1.228
largest diff. peak and hole (fm Å^{-3})	0.783 and -0.984

R1 [a] = $\Sigma \mid \mid F_o \mid - \mid Fc \mid \mid / \Sigma \mid F_o \mid$. $wR2$ [b] = $\{\Sigma[w(F_o^2 - F_c^2)^2]/\Sigma[w(F_o^2)^2]\}^{1/2}$.